Control of spin diffusion and suppression of the Hanle oscillation by the coexistence of spin and valley Hall effects in Dirac materials

Xian-Peng Zhang, Chunli Huang, and Miguel A. Cazalilla

Phys. Rev. B **99**, 245106 — Published 5 June 2019

DOI: 10.1103/PhysRevB.99.245106

Control of Spin Diffusion and Suppression of the Hanle Oscillation by the Coexistence of Spin and Valley Hall Effects in Dirac Materials

Xian-Peng Zhang,[1,2] Chunli Huang,[3] and Miguel A. Cazalilla[1,4,5]

[1] *Donostia International Physics Center (DIPC), Manuel de Lardizabal, 4. 20018, San Sebastian, Spain*
[2] *Centro de Fisica de Materiales (CFM-MPC), Centro Mixto CSIC-UPV/EHU, 20018 Donostia-San Sebastian, Basque Country, Spain*
[3] *Department of Physics, The University of Texas at Austin, Austin, Texas 78712, USA*
[4] *Department of Physics, National Tsing Hua University, Hsinchu 30013, Taiwan*
[5] *National Center for Theoretical Sciences (NCTS), Hsinchu 30013, Taiwan*

In addition to spin, electrons in many Dirac materials possess an additional pseudo-spin degree of freedom known as 'valley'. In materials where the spin and valley degrees of freedom are weakly coupled, they can be both excited and controlled independently. In this work, we study a model describing the interplay of the spin and valley Hall effects in such two-dimensional materials. We demonstrate the emergence of an additional longitudinal neutral current that is both spin and valley polarized. The additional neutral current allows to control the spin density by tuning the magnitude of the valley Hall effect. In addition, the interplay of the two effects can suppress the Hanle oscillation, that is, the oscillation of the nonlocal resistance of a Hall bar device with in-plane magnetic field. The latter observation provides a possible explanation for the absence of the Hanle oscillation in a number of recent experiments. Our work also opens the possibility to engineer the conversion between the valley and spin degrees of freedom in two-dimensional materials.

I. INTRODUCTION:

Spin-orbitronics [1–5] and valleytronics [6–9] aim at manipulating internal degrees of freedom of Bloch electrons, which can have applications in low-energy consumption electronics and quantum computation. Some two-dimensional (2D) materials such as transition metal dichalcogenides (TMD) [10,11] are known to exhibit large spin-orbit coupling (SOC), whilst for others like graphene, it has been predicted that SOC can be enhanced by means of decoration with various types of absorbates[12–15] or by proximity to a substrate such as a TMD material[16–19]. Both intrinsic and extrinsic SOC can lead to the spin Hall effect (SHE), i.e. the generation of a spin current perpendicular to the applied electric field.

In many 2D materials Bloch electrons are endowed with an additional pseudo-spin degree of freedom known as 'valley'. The latter is related to the existence of independent high symmetry points in the Brillouin zone where the band structure exhibits degenerate Dirac points or extrema[20–23]. Analogous to the SHE, these systems are capable of exhibiting the so-called valley Hall effect (VHE)[24–27], i.e. the appearance of a transverse valley-polarized bulk current in response to the application of an external electric field. Indeed, symmetry considerations imply that spin and valley are coupled in materials with broken spin-rotation and/or inversion symmetry. As such, 2D materials and van der Walls heterostructures have emerged as some of the most promising platforms to investigate this interesting interplay of spintronics and valleytronics. While spin and valley currents are electrically neutral, both currents carry angular momentum. In pristine graphene where SOC is negligible, valley current carries orbital angular momentum

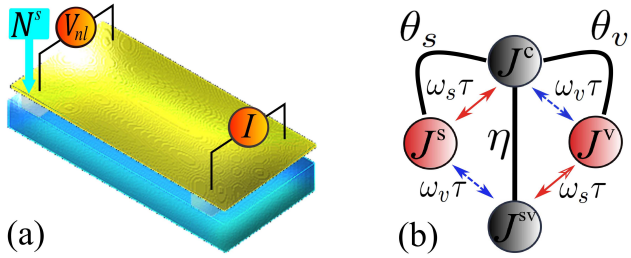

FIG. 1. (a) Sketch of a Hall-bar device used for measuring the nonlocal resistance R_{nl}: A current I is injected on one side and a (non local) voltage V_{nl} is detected in the opposite side. The nonlocal resistance is defined as $R_{nl} \equiv V_{nl}/I$. In this work, we assume that the spin and valley Hall effect coexist in the device. (b) Sketch of the four types of current response described by our model. Unlike the longitudinal electric (charge) current (J^c), the transverse spin (J^s) and valley (J^v) currents and the longitudinal spin-valley (J^{sv}) current are all electrical neutral and therefore cannot be detected by all electrical means. In the absence of SHE (VHE), $\omega_v\tau$ ($\omega_s\tau$) determines the conversion rate from J^c to J^v (J^s). However, when both SHE and VHE are present, J^{sv} mediates a coupling between J^s and J^v, which has important consequences for the spin-diffusion as shown on the spin density of Fig. 2(a).

while spin current carries spin angular momentum. In the opposite limit, in TMDs, for which the spin-momentum locking SOC is strong, there is often no distinction between the two.

Being electrically neutral, direct detection of spin and valley currents is not possible and their existence must be inferred by indirect means such as nonlocal transport measurements performed on a Hall bar device as depicted

in Fig. 1(a). In this setup, spin/valley currents are generated by driving an electric current between the two opposite right hand side contacts of the device. The neutral (spin/valley) currents diffuse in the transverse direction to the applied electric current (field), leading to a charge accumulation and a nonlocal voltage on the left hand side of the device. The nonlocal resistance (NLR) is defined as the ratio of the nonlocal voltage, V_{nl} to the external current applied to the device, I. Using this setup, the VHE has been experimentally observed in devices made by depositing monolayer graphene on hexagonal boron nitride (hBN)[25], bilayer graphene in a perpendicular displacement field[28], as well as optically pumped TMDs[29–32]. Likewise, the SHE has been experimentally observed in graphene decorated with absorbates[33–36] and graphene-TMDs heterostructures[37–39].

In connection to the observation of the SHE, the Hanle oscillation (HO), i.e. the modulation of the NLR as a function of an in-plane magnetic field is considered to be the hallmark of the existence of spin currents[33,34,40,41]. However, the absence of HO in some experiments in which a large enhancement of the NLR was observed[42–44] hints at the existence of additional contributions to the NLR that are insensitive to the magnetic field. One candidate that can contribute to the NLR is a valley current, which, as we have shown elsewhere[27], can arise from a modest amount of nonuniform strain present in the Hall bar device.

Previous theoretical studies of nonlocal transport have focused either on the VHE[26,27,45] or the SHE[40,41]. Building upon and largely extending earlier work, here we study the interplay between the two effects. In connection to the experiments described above, we show that this interplay can have nontrivial consequences for the spin transport in 2D materials. For instance, we find that spin density along the Hall bar can be modulated by the coupling between spin and valley currents, which can be controlled by the application of a nonuniform strain to the device[27]. This provides an exciting link between spintronics and straintronics[46–49]. In addition, we find that the HO can be strongly suppressed by the interplay with the VHE, and even absent under some circumstances. This finding can reconcile the apparently contradictory experimental results of various groups[43,44,50], some of which have observed a large enhancement of the NLR but failed to observe the HO[43,44]. Thus, the study reported here can be useful in guiding future studies of nonlocal transport in graphene, TMDs, and other 2D materials.

II. THEORY

We shall work in the diffusive regime where $k_F\ell \gg 1$, k_F being the Fermi momentum of the electrons and ℓ the elastic mean-free path. This is the relevant regime to the devices that are experimentally studied (e.g. Refs.[33,34,43,44,50]). In this regime, the transport of spin and valley degrees of freedom can be described by a set of drift-diffusion equations. In the steady state, the equations take the following generic structure:

$$\mathcal{D}\partial_i N^\mu - \sigma_D E_i^\mu = \left[-\delta^\mu_\nu \delta_{ij} + (R_H)^\mu_\nu\, \epsilon_{ij}\right] J^\nu_j. \qquad (1)$$

Here, we have used the convention that repeated indices are summed over. The Latin indices correspond to the spatial component of the current, or field, i.e. $\{i,j\} \in \{x,y\}$ and ϵ_{ij} is the antisymmetric 2D Levi-Civita tensor. The Greek indices of the currents, $\boldsymbol{J}^\mu$, and densities, N^μ, take values from the set $\{c, sv, v, s\}$. The latter stand for charge (c), spin-valley (sv), valley (v), and spin (s) current (density) respectively. Assuming that the spin splitting energy is much smaller than τ^{-1}, where τ is the elastic scattering time, we have derived the above set of drift-diffusion equations from a quantum Boltzmann equation (see Appendix B for details). In this derivation, due to the co-existence of the valley and spin Hall effects, the spin-valley current $\boldsymbol{J}^{sv}$ and density N^{sv} appear naturally as hydrodynamic modes that must be treated on equal footing to the spin and valley currents. As it results from this derivation of Eq. (1), the coefficients $\sigma_D = ne^2\tau/m$ and $\mathcal{D} = v_F^2/2$ take the same value for all (charge, spin, and spin-charge) currents. It is expected that, for instance, Coulomb interaction (i.e. Fermi-liquid) effects [see e.g. Ref.[51]] can renormalize the coefficients $\mathcal{D}$ and σ_D such that they become different for charge, spin, valley, and spin-valley currents. We have neglected such renormalization effects and therefore we end up with the same coefficients σ_D and $\mathcal{D}$. Our theory can be easily extended to account for this kind of renormalization. However, such a study lies beyond the scope of the present work. Furthermore, even at the phenomenological level, accounting for the different values of $\mathcal{D}$ and σ_D will unnecessarily increase complexity the model.

The left hand side of Eq. (1) contains the driving terms that result from spatial non-uniformity of the densities $\propto \partial_i N^\mu$ and the generalized electric fields $\propto E_i^\mu$ (to describe real devices, we shall set $E_i^\mu = 0$ for all $\mu \neq c$). The right hand side of Eq. (1) describes the effective Lorentz forces as well as current relaxation. The Drude conductivity is $\sigma_D = ne^2\tau/m$ and the diffusion constant is $\mathcal{D} = v_F^2\tau/2$. Next, we introduce the coupling between different currents via the Hall resistivity matrix R_H which describes both SHE and VHE. The latter couples the charge (c, 1st row) and spin-valley currents (sv, 2nd row) to valley (v, 3rd row) and spin (s, 4th row) currents:

$$R_H = \begin{bmatrix} 0 & 0 & \omega_v\tau & \omega_s\tau \\ 0 & 0 & \omega_s\tau & \omega_v\tau \\ \omega_v\tau & \omega_s\tau & 0 & 0 \\ \omega_s\tau & \omega_v\tau & 0 & 0 \end{bmatrix} \begin{matrix} c \\ sv \\ v \\ s \end{matrix} \qquad (2)$$

The SHE (VHE) can be regarded as emerging from an effective spin (valley) dependent Lorentz force[27,29,52,53]. In R_H, the magnitude of such forces are parameterized by

the "cyclotron" frequencies ω_s and ω_v, for spin and valley, respectively. These forces can have their origin in intrinsic or extrinsic SOC for the SHE[2], and in nonuniform strain[27] or skew scattering with impurities in gapped (monolayer/bilayer) graphene (valley)[54,55]. In the latter case, we neglect intrinsic Berry-curvature contributions to the valley current, as they are subdominant in the limit where impurities are dilute[55]. Note that when the valley and spin Hall effects coexist, the effective Lorentz force driving the VHE (SHE) current will act on the spin (valley) current. This is described by the additional entries in the R_H which are not present when only the SHE or the VHE exist in the material (see Fig. 1(b)).

In order to describe spin-valley transport with the above equations, we invert the resistivity matrix R_H in the right hand side of Eq. (1) and solve for the currents J_i^μ:

$$J_i^\mu = -\left(D_{ij}\right)_\nu^\mu \partial_j N^\nu + \left(\sigma_{ij}\right)_\nu^\mu E_j^\nu. \tag{3}$$

Note that the diffusion matrix is a rank-2 tensor in the Latin indices i, j, and therefore it can be split into a symmetric ($\propto \delta_{ij}$) and antisymmetric ($\propto \epsilon_{ij}$) part according to $D_{ij} = D_0\delta_{ij} + D_H\epsilon_{ij}$, where

$$D_0 = \mathcal{D}_r \begin{bmatrix} 1 & \eta & 0 & 0 \\ \eta & 1 & 0 & 0 \\ 0 & 0 & 1 & \eta \\ 0 & 0 & \eta & 1 \end{bmatrix}, \tag{4}$$

$$D_H = \mathcal{D}_r \begin{bmatrix} 0 & 0 & \theta_v & \theta_s \\ 0 & 0 & \theta_s & \theta_v \\ \theta_v & \theta_s & 0 & 0 \\ \theta_s & \theta_v & 0 & 0 \end{bmatrix}, \tag{5}$$

$$\mathcal{D}_r = \mathcal{D}\frac{1 + (\omega_v\tau)^2 + (\omega_s\tau)^2}{[1 + (\omega_v\tau)^2 + (\omega_s\tau)^2]^2 - 4\omega_s\omega_v\tau^2}. \tag{6}$$

Similarly, a decomposition of conductivity matrix as $\sigma_{ij} = \sigma_0\delta_{ij} + \sigma_H\epsilon_{ij}$ can be obtained by replacing in the above expressions the diffusion constant $\mathcal{D}$ with the Drude conductivity σ_D. Note that the diffusion equation (3) involves an off-diagonal diffusion coefficient (cf. Eqs. 4 to 6) and conductivity, which reduces to the well known limits. Thus, it yields the spin diffusion equations for a 2D electron gas[53,56] when the second and third rows and columns of the diffusion matrix D vanish. However, when the entries of the second and fourth rows and columns of D vanish, Eq. (3) describes the diffusion of valley polarization.

In order to understand some of the physical consequences of the coupling of spin and valley Hall effect described by the above equations, let us first solve Eq. (3) in the spatial uniform case where $\partial_j N^\mu = 0$. The ratios of the induced current (spin-valley $\boldsymbol{J}^{sv}$, valley $\boldsymbol{J}^v$, spin current $\boldsymbol{J}^s$) over charge current $\boldsymbol{J}^c$ are the figures of merit for the various effects and they are denoted respectively as η, θ_s, θ_v; in particular, θ_s and θ_v are the spin Hall and valley Hall angles; η describes the conversion efficiency of the electric current to the spin-valley current, and it is given by the following expression:

$$\eta = -\frac{2\left(\omega_v\tau\right)\left(\omega_s\tau\right)}{1 + (\omega_v\tau)^2 + (\omega_s\tau)^2}. \tag{7}$$

Note that η is proportional to the product of $\omega_v\tau$ and $\omega_c\tau$, as therefore it is nonvanishing provided both SHE and VHE coexist. As shown in Fig. 1(b), the generation of the spin-valley current is a two-stage process requiring the generation of a spin (valley) current from driving electric current via the SHE (VHE). The resulting transverse current is then again deflected by the effective Lorentz force that causes the VHE (SHE) resulting in a *longitudinal* spin-valley current. The factor of two in Eq. (7) stems from the two possible routes by which this spin-valley conversion can take place: charge to spin to spin-valley and charge to valley to spin-valley (see Fig. 1(b)).

Furthermore, due to the spin-valley interplay, the valley (θ_v) and spin Hall (θ_s) angles are modified as follows:

$$\theta_v = \frac{1 + (\omega_v\tau)^2 - (\omega_s\tau)^2}{1 + (\omega_v\tau)^2 + (\omega_s\tau)^2}\,\omega_v\tau, \tag{8}$$

$$\theta_s = \frac{1 + (\omega_s\tau)^2 - (\omega_v\tau)^2}{1 + (\omega_v\tau)^2 + (\omega_s\tau)^2}\,\omega_s\tau. \tag{9}$$

As expected, the spin (valley) Hall angle reduces to the familiar form $\theta_s = \omega_s\tau$ ($\theta_v = \omega_v\tau$) only when $\eta \propto \omega_s\omega_v = 0$. However, in general θ_s (θ_v) deviates from their "bare" values due to the interplay of the spin and valley Hall effects. In typical spintronic materials, $\omega_s\tau \ll 1$[2]. However, nonuniform strain in graphene [27], for instance, can yield large values of the (bare) Hall angles for which $|\omega_v\tau| \sim 1$. In this case, $|\theta_s| \sim |\omega_s\tau|^3 \ll 1$ implying that the spin current will be strongly suppressed (see discussion in the following section).

III. CONTROL OF SPIN DIFFUSION BY MEANS OF STRAIN

Next, we study the consequences of the interplay between spin and valley Hall effects for the spin transport in experimentally relevant devices. We first derive the drift-diffusion equations by supplementing Eq. (1) with the steady-state continuity equations for the currents, i.e. $\partial_i J_i^\mu = -\delta_\nu^\mu(\tau^\nu)^{-1}N^\nu$, where the limit $\tau^\mu \to +\infty$ for $\mu = c$ must be taken since the electric current is strictly conserved. Hence,

$$\left[\left(D_0\right)_\nu^\mu \nabla^2 - \frac{\delta_\nu^\mu}{\tau^\nu}\right] N^\nu = S^\mu. \tag{10}$$

In the above equations, τ^ν are the relaxation times of the various currents.[57] We have also assumed that spin-charge conversion mechanisms like the Edelstein effect or the direct magneto-electric coupling[40,56] can be neglected in a first approximation. S^μ is a source term given by

$$S^\mu = \epsilon_{ij}\left[-\partial_i\left(D_H\right)_\nu^\mu \partial_j N^\nu + \partial_i\left(\sigma_H\right)_\nu^\mu E_j^\nu\right]. \tag{11}$$

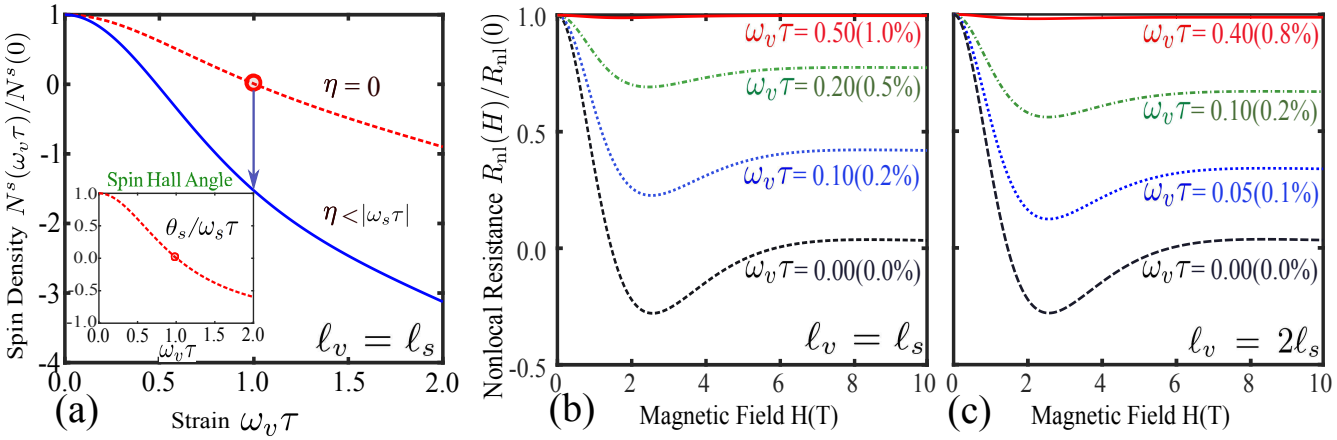

FIG. 2. (Color online) (a) Spin polarization, $N^s(x)$ at $x = 2\,\mu$m for a Hall bar device of width $w = 0.5\,\mu$m versus $\omega_v\tau$, which is controlled by the non-uniform strain applied to the device (τ is mean elastic collision time). The red dotted line is plotted by artificially setting the coupling η that controls the interplay of spin and valley to zero. Notice that ignoring the interplay when solving the diffusion equations (cf. Eq. 12) results in a substantial difference in the value of the spin-density diffusing along a Hall bar device. The inset shows the spin Hall angle θ_s from Eq. (9) normalized to $\omega_s\tau \simeq -0.12$. Notice that a modest nonuniform strain can lead to a large valley Hall effect[27], $\omega_v\tau(\gtrsim 1)$. $\omega_v\tau = 1$ can be induced by e.g. applying a nonuniform (uniaxial) strain of 2.0% to a ribbon of width $w = 0.50\mu$m. Panels (b) and (c) show the nonlocal resistance $R_{nl}(x, H)$ (normalized to $R_{nl}(x, H = 0)$) plotted versus the in plane magnetic field H for two different values of the ratio of the valley to spin diffusion lengths: (b) for $\ell_v = \ell_s$ and (c) for $\ell_v = 2\ell_s$. Parameters: $\ell_s = 0.53\,\mu$m, $x = 2.00\,\mu$m and $y = 0.25\,\mu$m.

Note that S^μ vanishes in the bulk of the Hall bar device, and it is only nonzero wherever D_H and σ_H are discontinuous, i.e. at the boundary. Thus, away from the boundaries, D_H and σ_H become constant and Eq. (10) can be written as follows:

$$\nabla^2 N^\mu - \mathcal{M}^\mu_\nu N^\nu = 0, \tag{12}$$

where

$$\mathcal{M}^\mu_\nu = \frac{1}{1-\eta^2}\begin{bmatrix} \ell_v^{-2} & -\eta\ell_s^{-2} \\ -\eta\ell_v^{-2} & \ell_s^{-2} \end{bmatrix} \begin{matrix} v \\ s \end{matrix}. \tag{13}$$

Only spin and valley densities are considered in the above equations because they are the only responses in the transverse direction to the applied electric field. In this expression, $\ell_v = \sqrt{\mathcal{D}_r\tau^v}$ ($\ell_s = \sqrt{\mathcal{D}_r\tau^s}$) is valley (spin) relaxation length and $\mathcal{D}_r$ is the (renormalized) diffusion constant (cf. Eq. 6). Note that the off-diagonal terms proportional to η mix the spin and valley densities. Eq. (12) is solved by first finding the eigenvalues and eigenvectors of the diffusion matrix, i.e. $\mathcal{M}^\mu_\nu|\hat{\boldsymbol{e}}^\nu_a\rangle = \mathcal{L}_a^{-2}|\hat{\boldsymbol{e}}^\mu_a\rangle$, where $\mathcal{L}_a$ ($a = 1, 2$) corresponds to the diffusion length of the eigenvector $|\hat{\boldsymbol{e}}^\mu_a\rangle$.

In order to illustrate the properties of the solution to the above diffusion equations, we consider a nonuniformly strained graphene device decorated with absorbates that locally induce SOC. As mentioned above, this system can be relevant to the experiments reported in Refs.[43,44]. In the long wave-length limit, the effect of nonuniform strain can be described by a out-of-plane (orbital) pseudo-magnetic field, which takes opposite signs at opposite valleys[27,46,47]. In earlier work, we have shown that modest amounts of nonuniform strain can lead to a sizable VHE[27]. In addition, skew scattering with the absorbates induces the SHE[33,53,58,59]. Thus, in this system both VHE and SHE coexist and the spin and valley transport is described by Eq. (12), whose solution we shall analyze in what follows.

For the sake the simplicity, we take the Hall bar to be an infinitely long conducting channel of width w[26,41]. The solution of the coupled diffusion equations is simplified by setting $N^c(\boldsymbol{r}) = 0$, which results from assuming the complete screening of the electric field inside the metal. Thus, the electrostatic potential $\Phi(\boldsymbol{r})$ obeys the Laplace equation, i.e. $\nabla^2\Phi(\boldsymbol{r}) = 0$. Using the appropriate boundary conditions[26,27], the valley and spin densities, at the edge ($y = \pm w/2$), are given by the following expression:

$$N^\mu(x) = \frac{iI}{\mathcal{D}_r}\sum_{\nu,b}\hat{\boldsymbol{e}}^\mu_b(\hat{\boldsymbol{e}}^{-1})^b_\nu\theta_\nu\int_{-\infty}^{\infty}\frac{dk}{2\pi k}\frac{e^{ikx}\mathcal{F}_b(k)}{1+\sum_a\Theta^2_a\mathcal{F}_a(k)},$$
$$\mathcal{F}_a(k) = \frac{k\tanh(kw/2)}{\kappa_a\tanh(\kappa_a w/2)}, \tag{14}$$

with $a, b = (1, 2)$; $\mu = v, s$ correspond to valley and spin densities, respectively. $\kappa_a = \sqrt{k^2 + \mathcal{L}_a^{-2}}$ and $\Theta^2_a = [\hat{\boldsymbol{e}}^\mu_a\theta_\mu]\,[(\hat{\boldsymbol{e}}^{-1})^\nu_a\theta_\nu]$.

Using the above solution, we show in what follows that the spin polarization diffusing in the Hall bar can be controlled by the application of nonuniform strain. In Fig. 2(a), we plot the spin polarization $N^s(x, y)$ (taking $x = 2\,\mu$m and $y = 0.25\,\mu$m) as a function of the $\omega_v\tau$, which is determined by the strength of the pseudo-

magnetic field induced by the nonuniform strength applied to device[27]. Interestingly, the spin polarization does not vanish even when the strain is tuned to make the effective spin Hall angle (cf. Eq. (9)) $\theta_s = 0$ (see red circle in the inset of Fig. 2(a)). This is a dramatic consequence of the coupling between the SHE and VHE, whose strength is measured by η (cf. Eq. (7)). Due to this coupling, the valley density accumulation induced by VHE can be converted to spin density. Note that if we solve the diffusion equations by ignoring the spin-valley coupling (i.e. by artificially setting the parameter $\eta = 0$ in Eq. 14) the behavior of the spin polarization (red line in Fig. 2(a)) would be very different.

IV. HANLE OSCILLATION

Finally, we show that the interplay between the SHE and VHE can lead to the suppression of the Hanle oscillation (HO). As mentioned above, the quantity of experimental interest is the NLR of the Hall bar measured at distance x from the current injection point. The HO results in the appearance of an oscillatory component in the NLR as a function of the external magnetic field H applied in the plane of the device. The oscillation is the result of the precession of the electron spins in the external magnetic field H.

By solving the coupled diffusion and Laplace equations, the NLR can be obtained from:

$$R_{nl}\left(x,H\right)=\frac{1}{I}\left[\Phi\left(x,-\frac{w}{2},H\right)-\Phi\left(x,\frac{w}{2},H\right)\right] \quad (15)$$

where $\Phi(x,y,H)$ is the electrostatic potential for an in-plane magnetic field H. In the absence of both SHE and VHE, the NLR is given by the van der Paw law: $R^0_{nl} \simeq \frac{4}{\pi\sigma^c}e^{-|x|/\mathcal{L}_0}$, for $|x| \gg \mathcal{L}_0 = w/\pi$. However, experimentally it is found[33,34,40,43] that the NLR is greatly enhanced with respect to the *Ohmic* signal. When the spin-diffusion length ℓ_s is shorter than the valley-diffusion length, ℓ_v, a suppression of the HO is expected. This is because the valley currents, which diffuse much farther and therefore will yield the dominant contribution to $R_{nl}(x,H)$, are completely insensitive to the in-plane magnetic field. Strikingly, we find that for ℓ_v and ℓ_s take comparable values, the HO can be suppressed by a moderate amount of nonuniform strain present in the device.

In order to compute $R_{nl}(x,H)$ we add to the diffusion equations (10), a Zeeman term, which induces precession. A magnetic field $\boldsymbol{H} \propto \hat{\mathbf{y}}$ converts the out-of-plane spin polarization, $N^s(x)$, into an in-plane spin polarization (along the x-direction). Since the nonlocal voltage is determined by the magnitude of $N^s(x)$ at the location the voltage probes (see Appendix C), this results in the NLR developing an oscillatory component. When the SHE and VHE coexist, describing precession requires that we account for the diffusion of the components of the spin and spin-valley densities in the plane perpendicular to $\boldsymbol{H}$. The solution of the resulting diffusion equations becomes more involved and the details are provided in the Appendix D. Here we focus on the discussion of the result for the NLR, which is shown in Fig. 2(b,c). The origin of the suppression described below can be traced back to the solution of the drift-diffusion equations. We find there are multiple diffusion eigenmodes which do not have a pure spin or valley character (i.e. they are mixed). The eigenmodes also possess different (complex) diffusion eigenlengths and thus yield different contributions to the nonlocal resistance in response to the precession induced by the applied magnetic field.

In Fig. 2(b), the NLR versus the applied magnetic field H has been plotted for $\ell_v = \ell_s$. Setting $\omega_v\tau = 0$, we recover the result obtained by Abanin *et al.*[41], showing the characteristic oscillatory component in $R_{nl}(x,H)$ associated with the HO. As the nonuniform strain (i.e. $\omega_v\tau$) in the Hall bar increases, the amplitude of the oscillatory component in the NLR is suppressed and almost disappears for $\omega_v\tau \sim 0.5$, which, for typical experimental parameters[43], corresponds to a nonuniform (uniaxial) strain of $\approx 1\%$ applied to a Hall bar 0.5 μm wide. For larger valley diffusion length ($\ell_v = 2\ell_s$), the suppression of the HO becomes even more obvious and happens for smaller amount of strain, as shown in Fig. 2(c). In the Appendix D we show that the suppression of the HO is not affected by charging the carrier density or sign. Notice that small to moderate amounts of nonuniform strain could be unintentionally introduced during the process of device fabrication. Thus, our findings are relevant for the interpretation of some of the nonlocal transport measurements in graphene decorated with hydrogen[44] and gold adatoms[43], where a large enhancement of the NLR was detected without HO.

Before concluding, it is worth commenting on other possible causes for the suppression of the HO. Indeed, suppression of the effect may also arise from a sizable spin-valley locking such as the one present in the band structure of TMDs[60]. Effectively, this type of spin-valley locking can be described as a Zeeman coupling to an out-of-plane magnetic field which takes opposite signs at opposite valleys. However, in graphene devices, such type of spin-valley would require breaking the sub lattice symmetry, which can be induced by either the substrate or the absorbates decorating the device. However, such a strong sublattice symmetry breaking was not experimentally observed[43]. The strong spin-valley coupling resulting from the spin-orbit coupling in TMDs will substantially modify the present theory. In particular, we can expect that the spin and valley currents will no longer be independent due to the large spin-orbit splitting, which effectively locks the valley and spin degrees of freedom. This also means that the spin-valley current will become irrelevant in such a theory.

V. SUMMARY AND OUTLOOK

We have explored a number of physical consequences of a simple models describing the coexistence of spin and valley Hall effects in two-dimensional materials: We have shown the latter leads to the emergence of neutral longitudinal spin and valley polarized current. Furthermore, we have shown the spin polarization diffusing in the material can be controlled by means of nonuniform strain. Finally, we have shown the Hanle effect in response to an in-plane magnetic field can be strongly suppressed due to the competition of the two effects. We believe the suppression of the Hanle effect noticed here will shed light on experimental controversies concerning the origin of the enhancement of the nonlocal resistance in various types of graphene devices [33,34,43,44,50]. The theory presented here can also be extended in various other directions, such as accounting for other spin-charge conversion mechanisms beyond the SHE (such as the inverse spin-galvanic effect) and a weak spin-valley (Zeeman) coupling, which is present in hybrid graphene-TMD structures. Both effects are expected to be important when spatial inversion symmetry is broken.

ACKNOWLEDGMENTS

This work is supported by the Ministry of Science and Technology (Taiwan) under contract number NSC 102- 2112-M-007-024-MY5 (MAC and CH), the Spanish Ministerio de Economía y Competitividad (MINECO) through Project No. FIS2014-55987-P and FIS2017-82804-P (XP and CL), and Taiwan's National Center of Theoretical Sciences (MAC and CL). We thank F. Guinea, A. Kaverzin, and R. Stephen for useful discussions.

Appendix A: Kinetic theory

1. Boltzmann equation

In this subsection, we introduce a quantum Boltzmann equation (QBE) capable of describing a system in which both spin (SHE) and valley Hall (VHE) effects co-exist:

$$\dot{n}_{\boldsymbol{k}} + \boldsymbol{v}^{\boldsymbol{k}} \cdot \nabla_{\boldsymbol{r}} n_{\boldsymbol{k}} + \boldsymbol{F}_{\boldsymbol{k}} \cdot \nabla_{\boldsymbol{k}} n_{\boldsymbol{k}} + i\omega_L \left[n_{\boldsymbol{k}}, \boldsymbol{s} \cdot \boldsymbol{m} \right] = \mathcal{I}_r \left[n_{\boldsymbol{k}} \right]. \tag{A1}$$

In the above expression, the function $n_{\boldsymbol{k}}$ is the density-matrix distribution function of the carriers (electrons or holes) in the Bloch state characterized by (crystal) momentum $\boldsymbol{k}$. Thus, it is a 4×4 matrix in spin-valley space. The force $\boldsymbol{F}$ driving the carrier motion can be split into three terms:

$$\boldsymbol{F}_{\boldsymbol{k}} = \boldsymbol{F}^l_{\boldsymbol{k}} + \boldsymbol{F}^s_{\boldsymbol{k}} + \boldsymbol{F}^v_{\boldsymbol{k}}, \tag{A2}$$

where

$$\boldsymbol{F}^l_{\boldsymbol{k}} = \boldsymbol{F}^E_{\boldsymbol{k}} + \boldsymbol{F}^B_{\boldsymbol{k}} \equiv e\boldsymbol{E} + e\boldsymbol{v}^{\boldsymbol{k}} \times \boldsymbol{B}, \tag{A3}$$

$$\boldsymbol{F}^s_{\boldsymbol{k}} = e\boldsymbol{v}^{\boldsymbol{k}} \times (\hat{s}_z \boldsymbol{\mathcal{B}}_s), \tag{A4}$$

$$\boldsymbol{F}^v_{\boldsymbol{k}} = e\boldsymbol{v}^{\boldsymbol{k}} \times (\hat{\tau}_z \boldsymbol{\mathcal{B}}_v). \tag{A5}$$

The $F^l_{\boldsymbol{k}}$ is the electromagnetic Lorentz force due to external (in-plane) electric and (out-of-plane) magnetic fields ($\boldsymbol{E} \perp \hat{\boldsymbol{z}}$ and $\boldsymbol{B} \parallel \hat{\boldsymbol{z}}$, respectively). While $F^{s/v}_{\boldsymbol{k}}$ are the effective (Lorentz-like) forces for effective (out-of-plane) spin/valley magnetic field ($\boldsymbol{\mathcal{B}}_s \parallel \hat{\boldsymbol{z}}$ and $\boldsymbol{\mathcal{B}}_v \parallel \hat{\boldsymbol{z}}$, respectively), from which the SHE and VHE originate. In Eq. (A3), $e(<0)$ is the charge of the electron, $\boldsymbol{v}^{\boldsymbol{k}} = \hbar^{-1}\nabla_{\boldsymbol{k}}\epsilon_{\boldsymbol{k}}$ is the velocity of electron with (crystal) momentum $\boldsymbol{k}$, and $\epsilon_{\boldsymbol{k}}$ is the band dispersion. We assume that there is no Berry curvature in the band and therefore anomalous velocity vanishes. $\hat{s}_a$, $\hat{\tau}_a$ $(a = o, x, y, z)$ are Pauli matrices describing the spin and valley (pseudospin), respectively. The matrix s_o (τ_o) corresponds to the spin (valley) unit matrix.

The magnitude of the SHE (VHE) has been parameterized in the above equations by the effective spin (valley) magnetic field $\hat{s}_z\boldsymbol{\mathcal{B}}_s$ ($\hat{\tau}_z\boldsymbol{\mathcal{B}}_v$), which points in opposite directions for electrons of different spins (valleys). The last term of the left hand side of Eq. (A1) describes spin precession with a Larmor frequency $\omega_L = g\mu_B H/\hbar$, which is proportional to the magnitude of the total applied (Zeeman) magnetic field $\boldsymbol{H}$ (g is the gyromagnetic factor and μ_B is the Bohr magneton). In Eq. (A1), $\boldsymbol{m} = \boldsymbol{H}/H$ denotes the direction of the total magnetic field and $\boldsymbol{B}$ in Eq. (A3) denotes the component of the magnetic field perpendicular to the plane of the material. In what follows, we shall assume that the external magnetic field (when present) is applied in the plane of the 2D system, which means $\boldsymbol{B} = 0$ and therefore the magnetic field part of Lorentz force $\boldsymbol{F}^B_{\boldsymbol{k}} = 0$.

On the right hand side of Eq. (A1) $\mathcal{I}_r\left[n_{\boldsymbol{k}}\right]$ is the (dissipative) collision integral. Strictly speaking, the force terms proportional to $\boldsymbol{F}^{s/v}_{\boldsymbol{k}}$ can arise from the collision integral as a result of skew scattering (see A 3 below and e.g. Refs.[27,53]). Alternatively, a weak uniform (i.e. intrinsic) Rasbha-type SOC can also give rise to a Lorentz-like force term like $\boldsymbol{F}^s_{\boldsymbol{k}}$ in the QBE[56,61]. Furthermore, nonuniform strain can give rise to a force like $\boldsymbol{F}^v_{\boldsymbol{k}}$ (see below, A 3, and Ref.[27]).

2. Linearized Boltzmann equation

For small applied electric field, $\boldsymbol{E}$, the solution to the QBE (A1), can be obtained by using the following ansatz for electron density-matrix distribution function:

$$n_{\boldsymbol{k}}(\boldsymbol{r}, t) = n^0\left[\epsilon_k - \mu_F - \gamma_\nu(\mu^\nu(\boldsymbol{r}, t) + \boldsymbol{v}^\nu(\boldsymbol{r}, t)\cdot\boldsymbol{k})\right]. \tag{A6}$$

In the above equation, $n^0(\epsilon)$ is Fermi-Dirac distribution at the absolute temperature T and global chemical potential μ_F. The convention of summing over repeated

Greek indices like ν has been used, with matrix γ_ν belonging to the set of 4×4 matrices $\{\hat{s}_o,\hat{s}_z\}\otimes\{\hat{\tau}_o,\hat{\tau}_z\} = \{\hat{s}_o\hat{\tau}_o,\hat{s}_o\hat{\tau}_z,\hat{s}_z\hat{\tau}_o,\hat{s}_z\hat{\tau}_z\}$, which are a set of 4×4 matrices in spin-valley space. The index ν runs over the combinations for charge ($c = oo$), spin-valley ($sv = zz$), valley ($v = oz$) and spin ($s = zo$) indices. The fields $\boldsymbol{v}^\nu(\boldsymbol{r},t)$ and $\mu^\nu(\boldsymbol{r},t)$ correspond to the drift velocity of the electron fluid and the local chemical potential, respectively. Both are proportional to applied electric field, i.e., $|\boldsymbol{v}^\nu(\boldsymbol{r},t)| \propto |\boldsymbol{E}|$ and $\mu^\nu(\boldsymbol{r},t) \propto |\boldsymbol{E}|$. To linear order in $\boldsymbol{v}^\nu(\boldsymbol{r},t)$ and $\mu^\nu(\boldsymbol{r},t)$, the deviation of distribution function from its equilibrium, $\delta n_{\boldsymbol{k}} = n_{\boldsymbol{k}} - n^0_k$ reads:

$$\delta n_{\boldsymbol{k}}(\boldsymbol{r},t) \simeq \gamma_\nu\left[\mu^\nu(\boldsymbol{r},t) + \boldsymbol{v}^\nu(\boldsymbol{r},t)\cdot\boldsymbol{k}\right]\left[-\partial_\epsilon n^0_\epsilon\right]_{\epsilon=\mu_F}, \tag{A7}$$

with $\nu = (c, sv, v, s)$. Hence,

$$\nabla_{\boldsymbol{k}}\delta n_{\boldsymbol{k}}(\boldsymbol{r},t) \simeq \gamma_\nu \boldsymbol{v}^\nu(\boldsymbol{r},t)\left[-\partial_\epsilon n^0_\epsilon\right]_{\epsilon=\mu_F}. \tag{A8}$$

Thus, to linear order in $\boldsymbol{E}$, linearization of QBE yields:

$$\delta\dot{n}_{\boldsymbol{k}} + \boldsymbol{v}^{\boldsymbol{k}}\cdot\nabla_{\boldsymbol{r}}\delta n_{\boldsymbol{k}} + e\left(\boldsymbol{E}+\boldsymbol{v}^{\boldsymbol{k}}\times\boldsymbol{B}\right)\cdot\nabla_{\boldsymbol{k}}n^0_{\boldsymbol{k}} + \boldsymbol{F}^s_{\boldsymbol{k}}\cdot\nabla_{\boldsymbol{k}}\delta n_{\boldsymbol{k}} + \boldsymbol{F}^v_{\boldsymbol{k}}\cdot\nabla_{\boldsymbol{k}}\delta n_{\boldsymbol{k}} + i\omega_L\left[\delta n_{\boldsymbol{k}}, \boldsymbol{s}\cdot\boldsymbol{m}\right] = \mathcal{I}_r\left[\delta n_{\boldsymbol{k}}\right], \tag{A9}$$

where we have used:

$$\boldsymbol{F}^s_{\boldsymbol{k}}\cdot\nabla_{\boldsymbol{k}}n^0_{\boldsymbol{k}} \propto (\hat{\boldsymbol{k}}\times\hat{\boldsymbol{z}})\cdot\hat{\boldsymbol{k}} = 0, \tag{A10}$$

$$\boldsymbol{F}^v_k\cdot\nabla_{\boldsymbol{k}}n^0_{\boldsymbol{k}} \propto (\hat{\boldsymbol{k}}\times\hat{\boldsymbol{z}})\cdot\hat{\boldsymbol{k}} = 0, \tag{A11}$$

together with the vanishing of the collision integral for the equilibrium distribution n^0_k.

3. Example of a microscopic model

The above linearized QBE can be obtained for various types of microscopic models. In this subsection, we study an instance of much experimental interest describing a monolayer of graphene subject to nonuniform strain and decorated with adatoms. The latter induce spin-orbit coupling (SOC) by proximity to the graphene layer. For the sake of simplicity, the spatial dependence of SOC is approximated by a Dirac delta potential (but more complicated dependence will not alter our results qualitatively[58]). The spin-dependence corresponds to the so-called Kane-Mele SOC, which is known to lead to *extrinsic* SHE[53,58].

a. *Pseudo-magnetic field in strained graphene*

Within the $\boldsymbol{k}\cdot\boldsymbol{p}$ approximation to the band structure of graphene (see e.g.[20]), nonuniform (shear) strain can be described as a pseudo-gauge field which takes opposite signs at opposite valleys (see e.g.[20,46–48]):

$$H_0[\boldsymbol{k}-\hat{\tau}_z\boldsymbol{\mathcal{A}}(\boldsymbol{r})] = \hbar v_F\left[\hat{\tau}_z\hat{\sigma}_x(k_x - e\hat{\tau}_z\mathcal{A}_x) + \hat{\sigma}_y(k_y - e\hat{\tau}_z\mathcal{A}_y)\right]. \tag{A12}$$

In the above expression v_F is the Fermi velocity and σ_x,σ_y are the Pauli matrices describing the sublattice pseudo-spin. The pseudo-gauge $\boldsymbol{\mathcal{A}}(\boldsymbol{r})$ field which describes the (strain-induced) local displacement of the Dirac points at the two valleys is given by the following expression:

$$\boldsymbol{\mathcal{A}}(\boldsymbol{r}) = (\mathcal{A}_x,\mathcal{A}_y) = \tfrac{\beta}{ae}\left(u_{xx}-u_{yy}, -2u_{xy}\right), \tag{A13}$$

where $\beta = \frac{d\log t}{d\log a} \simeq 2$, t being the nearest neighbor hopping amplitude, a is the carbon-carbon distance, and

$$u_{ij} = \frac{1}{2}(\partial_i u_j + \partial_j u_i), \tag{A14}$$

is strain tensor. Note that, since u_{ij} is invariant (i.e. even) under time-reversal (TR) and $\hat{\tau}_z\boldsymbol{\mathcal{A}}(\boldsymbol{r})$ even under TR (recall that $\tau_z \to -\tau_z$ under TR). This is different from a real magnetic field, for which the gauge field is odd under TR.

The pseudo-magnetic field that determines the valley Lorentz-like force, $\boldsymbol{F}^v_{\boldsymbol{k}}$ can be obtained from the standard expression:

$$\hat{\tau}_z\boldsymbol{\mathcal{B}}_v = \hat{\tau}_z\nabla\times\boldsymbol{\mathcal{A}}(\boldsymbol{r}) = \hat{\tau}_z(\partial_x\mathcal{A}_y - \partial_y\mathcal{A}_x)\,\hat{\boldsymbol{z}}. \tag{A15}$$

Thus, as mentioned above, the pseudo-magnetic field $\hat{\tau}_z\boldsymbol{\mathcal{B}}_v$ induced by nonuniform strain has opposite signs at opposite valleys as required by the fact that strain does not break TR invariance. In what follows, for the sake of simplicity, we shall assume that the pseudo-magnetic field $\hat{\tau}_z\boldsymbol{\mathcal{B}}_v$ is spatially uniform, which requires particular configurations of nonuniform strain[27,46,48]. Thus, we have shown how strain can give rise to an effective Lorentz-like force $\boldsymbol{F}^v_{\boldsymbol{k}}$, which drives the VHE (alternatively, this force can emerge from skew scattering with scalar impurities in bands with nonzero Berry curvature[55]). Via the semi-classical equations of motion[11], the latter will enter the QBE in (A1).

b. *Adatom-induced SHE*

The spin transport properties of graphene can be modified by the presence of adatom impurities[35,53,58,59]. In the dilute impurity limit, the dominant mechanism for the spin-charge conversion via the extrinsic SHE is skew scattering[3], which effectively gives rise to a spin-dependent Lorentz-like force[53].

Within the $\boldsymbol{k}\cdot\boldsymbol{p}$ theory, the potential for a single-impurity takes the following form:

$$V(\boldsymbol{r}) = (\mathcal{V}_c\hat{s}_o\hat{\tau}_o\hat{\sigma}_o + \mathcal{V}_s\hat{s}_z\hat{\tau}_z\hat{\sigma}_z)R^2\delta(\boldsymbol{r}). \tag{A16}$$

In the above expression, R is a length scale of the order of the impurity radius. We shall assume that $R \gg a$, that is, much larger than the inter-carbon separation so that inter-valley scattering can be safely neglected[62] but $R \lesssim 10$ nm, so that the potential can be approximated by a Dirac δ-function. This approximation should be a good description of a monolayer of graphene decorated by adatom clusters[34,58]. Hence, upon solving the scattering problem, the on-shell T-matrix projected on the carrier band can be obtained and reads:

$$T^{+}_{\boldsymbol{kp}} = t_c(k)\hat{s}_o \cos(\theta_{\boldsymbol{kp}}/2) + t_s(k)\hat{s}_z \sin(\theta_{\boldsymbol{kp}}/2). \quad \text{(A17)}$$

The functions $t_c(k)$ and $t_s(k)$ depend on momentum k of the incoming electron and the impurity potential parameters, i.e. $\mathcal{V}_c, \mathcal{V}_s$, in our model. See e.g. Refs.[63] and[27] for the detailed expressions of these functions.

The effect of impurities is described by the collision integral $\mathcal{I}[\delta n_{\boldsymbol{k}}]$. The complete form of the latter (which includes the dissipative $\mathcal{I}_r[\delta n_{\boldsymbol{k}}]$ introduced in Eq. A1) has been derived in Ref.[63], extending earlier work of Kohn and Luttinger in order to account for the effects of disorder on the electron internal degrees of freedom such as spin and valley pseudo-spin. To leading order in the density of impurities, $n_{\rm i}$, the collision integral reads:

$$\mathcal{I}[\delta n_{\boldsymbol{k}}] = \frac{2\pi}{\hbar} n_{\rm i} \sum_{\boldsymbol{p}} \delta(\epsilon_k - \epsilon_p) \Big[T^{+}_{\boldsymbol{kp}} \delta n_{\boldsymbol{p}} T^{-}_{\boldsymbol{pk}} - \frac{1}{2} \Big\{ \delta n_{\boldsymbol{k}} T^{+}_{\boldsymbol{kp}} T^{-}_{\boldsymbol{pk}} + T^{+}_{\boldsymbol{kp}} T^{-}_{\boldsymbol{pk}} \delta n_{\boldsymbol{k}} \Big\} \Big], \quad \text{(A18)}$$

which is determined by the scattering data of a single scatterer. Using the above ansatz, Eq. (A7), the collision integral (A18) reduces to:

$$\mathcal{I}[\delta n_{\boldsymbol{k}}] = \frac{\pi}{\hbar} n_{\rm i} \sum_{\boldsymbol{p}} \delta(\epsilon_p - \epsilon_k)\, 2\hat{T}^{+}_{\boldsymbol{kp}} \hat{T}^{-}_{\boldsymbol{kp}} (\delta n_{\boldsymbol{p}} - \delta n_{\boldsymbol{k}}), \quad \text{(A19)}$$

where

$$2\hat{T}^{+}_{\boldsymbol{kp}} \hat{T}^{-}_{\boldsymbol{kp}} = \Big[|t_c|^2 (1+\cos\theta) + |t_s|^2 (1-\cos\theta) \Big] \gamma^c + 2\mathrm{Im}\,(t_c t_s^*) \sin\theta \gamma^s \quad \text{(A20)}$$

$$\delta n_{\boldsymbol{p}} - \delta n_{\boldsymbol{k}} = \big[-\partial_\epsilon n^0(\epsilon) \big]_{\epsilon=\mu_F} \sum_\nu \gamma^\nu \boldsymbol{v}^\nu(\boldsymbol{r}) \cdot \hbar(\boldsymbol{p}-\boldsymbol{k}). \quad \text{(A21)}$$

Substituting Eqs. (A20) and (A21) into Eq. (A18), the collision integral takes the following form:

$$\mathcal{I}[\delta n_{\boldsymbol{k}}] = \big[\partial_\epsilon n^0(\epsilon) \big]_{\epsilon=\mu_F} \hbar \boldsymbol{k} \cdot \Big\{ \frac{\gamma^c}{\tau} \sum_\nu \gamma^\nu \boldsymbol{v}^\nu(\boldsymbol{r}) + \gamma^s \omega_s \sum_\nu \gamma^\nu \boldsymbol{v}^\nu(\boldsymbol{r}) \times \hat{\boldsymbol{z}} \Big\}, \quad \text{(A22)}$$

where

$$\frac{1}{\tau(k)} = \frac{k n_{\rm i}}{4\hbar^2 v_F} \Big[|t_c(k)|^2 + 3\,|t_s(k)|^2 \Big], \quad \text{(A23)}$$

$$\omega_s(k) = \frac{k n_{\rm i}}{4\hbar^2 v_F} \left[-2\mathrm{Im}\{t_c(k) t_s(k)\} \right]. \quad \text{(A24)}$$

The above collision integral can be rewritten as

$$\mathcal{I}[\delta n_{\boldsymbol{k}}] = -\frac{\hbar \boldsymbol{k}}{\tau} \cdot \nabla_{\boldsymbol{k}} \delta n_k - \boldsymbol{F}^s_{\boldsymbol{k}} \cdot \nabla_{\boldsymbol{k}} \delta n_k, \quad \text{(A25)}$$

with

$$\boldsymbol{\mathcal{B}}_s = -\frac{\hbar k \omega_s}{e v_F} \hat{\boldsymbol{z}}. \quad \text{(A26)}$$

Thus, as anticipated in A 1 (cf. Eqs. (A1) and (A4)), an effective Lorentz-like force driving the SHE emerges from skew scattering with adatom impurities. This Lorentz-like force term needs to be factored out of the collision integral, and the remaining terms are grouped in the dissipative part of the the collision integral, $\mathcal{I}_r[n_{\boldsymbol{k}}]$, which we introduced in Eq. (A1), See A 1 .

Appendix B: Diffusion equations

In order to derive the diffusion equations that we have employed in the main text, let us first consider the simpler case where there is no applied magnetic field and therefore the Larmor frequency vanishes, i.e. $\omega_L = 0$ in Eq. (A9).

First of all, let us the define currents and generalized polarization densities as follows:

$$J^\nu_i = \sum_{\boldsymbol{k}} e v^{\boldsymbol{k}}_i \mathrm{Tr}\left[\gamma^\nu \delta n_{\boldsymbol{k}}\right], \quad \text{(B1)}$$

$$N^\nu = \sum_{\boldsymbol{k}} e \mathrm{Tr}\left[\gamma^\nu \delta n_{\boldsymbol{k}}\right]. \quad \text{(B2)}$$

At zero temperature, J^ν_i and N^ν reduce to:

$$J^\nu_i(\boldsymbol{r}) = e\nu_F \mu_F v^\nu_i(\boldsymbol{r}), \quad \text{(B3)}$$

$$N^\nu(\boldsymbol{r}) = 2e\nu_F \mu^\nu(\boldsymbol{r}), \quad \text{(B4)}$$

where $\nu_F = k_F^2/(\pi\mu_F)$ is the total density of states at the Fermi energy $\mu_F = \hbar v_F k_F$ at zero temperature, where k_F is the Fermi momentum.

1. Continuity and constitutive equations

The constitutive and continuity equations in steady state, can be obtained by tracing the linearized QBE (A9), i.e. by taking $\sum_{\boldsymbol{k}} e\boldsymbol{v}^{\boldsymbol{k}} \mathrm{Tr}\left[\gamma^\mu \mathrm{QBE}\right]$ for the constitutive equations and $\sum_{\boldsymbol{k}} e\mathrm{Tr}\left[\gamma^\mu \mathrm{QBE}\right]$) for the continuity relations, respectively. The latter procedures yield the following expressions:

$$\mathcal{D}\partial_i N^\mu - \sigma_D E^\mu_i = \left[-\delta^\mu_\nu \delta_{ij} + (R_H)^\mu_\nu \epsilon_{ij} \right] J^\nu_j, \quad \text{(B5)}$$

$$\partial_i J_i^\mu = 0. \tag{B6}$$

Here $\mathcal{D} = v_F^2\tau/2$ is diffusion constant and $\sigma_D = ne^2\tau/m$ (n is carrier density and m is mass) is Drude conductivity. In the above expression, repeated indices are summed and ϵ_{ij} is the antisymmetric 2D Levi-Civita tensor ($i, j = x, y$). The Greek superscripts of the currents $\boldsymbol{J}^\mu$ and the densities N^μ take values over the set $\{c, sv, v, s\}$, which stand for for charge, spin-valley, valley, and spin currents (densities), respectively. The coupling between spin and valley currents naturally leads to the existence of spin and valley polarized currents that are *longitudinal*, i.e. have the same direction as charge current $\boldsymbol{J}^c$(external electric field $\boldsymbol{E}^c = \boldsymbol{E}$). On the other hand, the spin and valley currents are *transverse*, i.e. perpendicular to $\boldsymbol{J}^c$ ($\boldsymbol{E}$).

The left hand side of Eq. (B5) contains the driving forces for the currents, which are the results of spatial nonuniformity of the densities $\propto \boldsymbol{\nabla} N^\mu$ and the application of the generalized electric fields $\boldsymbol{E}^\mu$ (in order to describe real devices, we shall set $\boldsymbol{E}^\mu = 0$ for all $\mu \neq c$). The right hand side of Eq. (B5) describes the effective Lorentz forces as well as current relaxation. The relaxation rates for all currents are the same and equal to the Drude relaxation time τ (which is related to the mean-free path by $\ell = v_F\tau$ where v_F is the Fermi velocity). The Hall resistivity matrix R_H describes SHE and VHE, and couples *longitudinal* charge and spin-valley currents to *transverse* spin and valley currents:

$$R_H = \begin{bmatrix} 0 & 0 & \omega_v\tau & \omega_s\tau \\ 0 & 0 & \omega_s\tau & \omega_v\tau \\ \omega_v\tau & \omega_s\tau & 0 & 0 \\ \omega_s\tau & \omega_v\tau & 0 & 0 \end{bmatrix}. \tag{B7}$$

The magnitude of the SHE and VHE has been parameterized in the above equations by the effective "cyclotron" frequencies

$$\omega_s = v_F e\mathcal{B}_s/\hbar k_F \tag{B8}$$

$$\omega_v = v_F e\mathcal{B}_v/\hbar k_F. \tag{B9}$$

The latter arise from effective Lorentz forces that deflect the electrons (according to their spin and valley orientations, respectively).

In order to describe spin-valley transport with the above equations, we need to invert the resistivity matrix R_H and solve Eq. (B5) for the currents J_i^μ, which yields the following set of equations:

$$J_i^\mu = -\left(D_{ij}\right)_\nu^\mu \partial_j N^\nu + \left(\sigma_{ij}\right)_\nu^\mu E_j^\nu. \tag{B10}$$

Note that the diffusion matrix is a rank-2 tensor in the Latin indices i, j, and therefore it can be split into a symmetric ($\propto \delta_{ij}$) and antisymmetric ($\propto \epsilon_{ij}$) part according to $D_{ij} = D_0\delta_{ij} + D_H\epsilon_{ij}$, where

$$D_0 = \mathcal{D}_r \begin{bmatrix} 1 & \eta & 0 & 0 \\ \eta & 1 & 0 & 0 \\ 0 & 0 & 1 & \eta \\ 0 & 0 & \eta & 1 \end{bmatrix}, \tag{B11}$$

$$D_H = \mathcal{D}_r \begin{bmatrix} 0 & 0 & \theta_v & \theta_s \\ 0 & 0 & \theta_s & \theta_v \\ \theta_v & \theta_s & 0 & 0 \\ \theta_s & \theta_v & 0 & 0 \end{bmatrix}, \tag{B12}$$

$$\mathcal{D}_r = \mathcal{D}\frac{1 + (\omega_v\tau)^2 + (\omega_s\tau)^2}{[1 + (\omega_v\tau)^2 + (\omega_s\tau)^2]^2 - 4\omega_s\omega_v\tau^2}. \tag{B13}$$

Similarly, a decomposition of conductivity matrix as $\sigma_{ij} = \sigma_0\delta_{ij} + \sigma_H\epsilon_{ij}$ can be obtained by replacing in the above expressions the diffusion constant $\mathcal{D}$ with the Drude conductivity σ_D. (See exact expressions for η, θ_v, θ_s in manuscript.)

2. Diffusion of spin and valley polarization

Next, we derive the drift-diffusion equations for the spin and valley polarizations. To this end, we supplement the constitutive relations in Eq. (B5) with the steady state phenomenological continuity equations,

$$\partial_i J_i^\mu = -\frac{\delta_\nu^\mu}{\tau^\nu} N^\nu, \tag{B14}$$

where we take $\tau^c \to +\infty$ since the charge current is strictly conserved. In the above expressions, τ^ν are phenomenological relaxation times which need to be *ad hoc* in the present derivation, but whose existence can be rigorously derived in a more complete treatment[27,63]. Hence, we arrive at the following set of diffusion equations:

$$\left[\left(D_0\right)_\nu^\mu \partial_i^2 - \frac{\delta_\nu^\mu}{\tau^\nu}\right] N^\nu = S^\mu, \tag{B15}$$

where the source term is given by

$$S^\mu = \epsilon_{ij}\left[-\partial_i \left(D_H\right)_\nu^\mu \partial_j N^\nu + \partial_i \left(\sigma_H\right)_\nu^\mu E_j^\nu\right]. \tag{B16}$$

In deriving the above diffusion equations, we used $\epsilon_{ij}\partial_i\partial_j N^\mu = 0$ and that the generalized electric field is curl and divergence-free, i.e. $\epsilon_{ij}\partial_i E_j^\mu = 0$ and $\partial_i E_i^\mu = 0$, that is, we have neglected any relativistic corrections to the electrodynamics.

Note that the source term on the right hand side of (B15) takes a non-zero values only at the boundary of the device. In other words, it describes the driving force for the electron diffusion arising from the abrupt change of the Hall angle at the device boundaries[26]. However, in the bulk the above set of differential equations (B15), becomes a homogeneous one:

$$\partial_i^2 N^\mu - \mathcal{M}_\nu^\mu N^\nu = 0, \tag{B17}$$

where

$$\mathcal{M}_\nu^\mu = \frac{1}{1-\eta^2}\begin{bmatrix} \ell_v^{-2} & -\eta\ell_s^{-2} \\ -\eta\ell_v^{-2} & \ell_s^{-2} \end{bmatrix}. \tag{B18}$$

Here $\mu,\nu \in \{v,s\}$ denote the transverse valley (spin) response, with diffusion lengths $\ell_v = \sqrt{\mathcal{D}_r\tau^v}$ ($\ell_s = \sqrt{\mathcal{D}_r\tau^s}$). The choice where $\mu,\nu = \{c, sv\}$ corresponds to the longitudinal charge (spin-valley) response, which decouples from transverse modes and will be omitted in what follows. The parameter η, which arises from the interplay of SHE and VHE, mixes the valley and spin responses.

As described in the main text, in order to solve Eq. (B17), we first need to diagonalize the matrix $\mathcal{M}$ and therefore obtain the eigenvalues and eigenvectors. Thus, in what follows we shall assume this has been carried out, so that $\mathcal{L}_a^{-2}|\hat{\boldsymbol{e}}_a^{\mu}\rangle = \mathcal{M}_{\nu}^{\mu}|\hat{\boldsymbol{e}}_a^{\nu}\rangle$, where $\mathcal{L}_a$ is the eigenvalue, which corresponds to the diffusion length for the eigenmode $|\hat{\boldsymbol{e}}_a^{\mu}\rangle$.

Next, following Beconcini *et al.*[26], we solve the diffusion equation for a Hall bar device geometry, assuming the latter to be an infinitely long metallic channel of width w contacted by noninvasive current and voltage probes (see Fig. 1(a) in the manuscript). We shall assume the complete screening of the electric field in the bulk of device, which amounts to take charge density into zero, i.e., $N^c(\boldsymbol{r}) = 0$. Hence, the electrostatic potential, $\Phi(\boldsymbol{r})$ obeys the Laplace equation:

$$\nabla^2\Phi(\boldsymbol{r}) = 0. \tag{B19}$$

The Laplace equation (B19) and the above system of partial differential equations (B17), need to be supplemented by the following boundary conditions (BCs):

$$J_y^c(x; y = \pm w/2) = I\delta(x) \tag{B20}$$

$$J_y^{\nu}(x; y = \pm w/2) = 0, \tag{B21}$$

for $\nu = v, s$. I is charge current injected on right hand side of Hall bar device. Finally, in order to solve the problem posed by Eq. (B17) and Eq. (B19), we use Fourier transformation along the infinitely long channel direction, x. Thus, using (B10), the BCs approximately become:

$$I \simeq \left[-\mathcal{D}_r\,(ik)\,N^{\nu}(k,y)\,\theta_{\nu} - \sigma^c\partial_y\Phi(k,y)\right]\big|_{y=\pm\frac{w}{2}}, \tag{B22}$$

where the sum over the repeated index ν in the expression above runs over the set $\{s,v\}$ only. σ^c is charge conductivity. In addition,

$$0 \simeq \left[-\sigma^c\,(ik)\,\Phi(k,y)\,\theta_{\nu} - \mathcal{D}_r\partial_y N^{\nu}(k,y)\right]\big|_{y=\pm\frac{w}{2}}. \tag{B23}$$

By "approximately", we mean that the boundary contributions of the longitudinal modes N^c and N^{sv} in Eq. (B10) have been omitted by setting $N^c, N^{sv} = 0$ and $\eta = 0$. Including them, merely leads to a small correction to the diffusion length of the spin and valley eigenmodes.

In order to solve the above system of 2nd order differential equations, i.e. Eq. (B17), we first turn it into a 1st order set of equations by defining $N'_{\nu}(k,y) = \partial_y N^{\nu}(k,y)$, rendering (B17) to the form:

$$\begin{bmatrix}\partial_y N^{\nu}(k,y)\\ \partial_y N'_{\mu}(k,y)\end{bmatrix} = \begin{bmatrix}0 & \delta_{\mu}^{\nu}\\ k^2\delta_{\nu}^{\mu} + \mathcal{M}_{\nu}^{\mu} & 0\end{bmatrix}\begin{bmatrix}N^{\nu}(k,y)\\ N'_{\mu}(k,y)\end{bmatrix}. \tag{B24}$$

Let $\mathcal{L}_a^{-2}$ and $|\hat{\boldsymbol{e}}_a^{\mu}\rangle$ are the eigenvalues and eigenvectors of diffusion matrix, respectively. Hence,

$$\begin{bmatrix}\mathbf{0} & \mathbb{1}\\ k^2\mathbb{1} + \mathcal{M} & \mathbf{0}\end{bmatrix}\begin{bmatrix}|\hat{\boldsymbol{e}}_a\rangle\\ \pm\kappa_a\,|\hat{\boldsymbol{e}}_a\rangle\end{bmatrix} = \pm\kappa_a\begin{bmatrix}|\hat{\boldsymbol{e}}_a\rangle\\ \pm\kappa_a\,|\hat{\boldsymbol{e}}_a\rangle\end{bmatrix}, \tag{B25}$$

with $\kappa_a = \sqrt{k^2 + \mathcal{L}_a^{-2}}$. Therefore, $\pm\kappa_a$ is the eigenvalue of the matrix of (B24) with eigenvector

$$|\pm\kappa_a\rangle = \frac{1}{(1+|\kappa_a|^2)^{1/2}}\begin{bmatrix}|e_a\rangle\\ \pm\kappa_a\,|e_a\rangle\end{bmatrix}. \tag{B26}$$

Considering the symmetry of BCs in (B22) and (B23), the solution of the above system of differential can be solved by the following ansatz:

$$N^{\nu} = \sum_{a=1,2} A_a\hat{\boldsymbol{e}}_a^{\nu}\left(e^{+\kappa_a y} + e^{-\kappa_a y}\right), \tag{B27}$$

$$\Phi = A_o\left(e^{+ky} - e^{-ky}\right). \tag{B28}$$

Substitution of these ansatz into the BCs, Eq. (B22) and (B23) yields:

$$I = -\sigma^c\left[A_o k\left(e^{+kw/2} + e^{-kw/2}\right)\right] - \mathcal{D}_r\sum_{\nu,a}\theta_{\nu}\,(ik)\left[A_a\hat{\boldsymbol{e}}_a^{\nu}\left(e^{+\kappa_a w/2} + e^{-\kappa_a w/2}\right)\right], \tag{B29}$$

$$0 \simeq -\sigma^c\theta_{\nu}\,(ik)\,A_o\left(e^{+kw/2} - e^{-kw/2}\right) - \mathcal{D}_r\sum_{a} A_a\hat{\boldsymbol{e}}_a^{\nu}\kappa_a\left(e^{+\kappa_a w/2} - e^{-\kappa_a w/2}\right). \tag{B30}$$

From Eq. (B30), it is found that

$$\frac{A_a}{A_o} \simeq (-i)\,\frac{\sigma^c}{\mathcal{D}_r}\sum_{\mu}\frac{k\sinh(kw/2)}{\kappa_a\sinh(\kappa_a w/2)}(\hat{\boldsymbol{e}}^{-1})_a^{\mu}\theta_{\mu}, \tag{B31}$$

Hence, upon substitution of this result into Eq. (B29), we obtain:

$$\frac{I}{A_o} = -2k\cosh\left(k\frac{W}{2}\right)\left[1+\sum_a \Theta_a^2\mathcal{F}_a\left(k\right)\right]\sigma^c, \tag{B32}$$

where

$$\Theta_a^2 = [\theta_\mu \hat{\boldsymbol{e}}_a^\mu][(\hat{\boldsymbol{e}}^{-1})_\nu^a\theta_\nu], \tag{B33}$$

$$\mathcal{F}_a\left(k\right) = \frac{k\tanh\left(kw/2\right)}{\kappa_a\tanh\left(\kappa_a w/2\right)}. \tag{B34}$$

Hence,

$$N^\nu\left(\boldsymbol{r}\right) = \frac{iI}{\mathcal{D}_r}\sum_{a,\mu}\hat{\boldsymbol{e}}_a^\nu(\hat{\boldsymbol{e}}^{-1})_\mu^a\theta_\mu\int dk\frac{e^{ikx}}{2\pi}\frac{\tanh\left(kw/2\right)}{\kappa_a\sinh\left(\kappa_a w/2\right)}\frac{\cosh\left(\kappa_a y\right)}{[1+\sum_b\Theta_b^2\mathcal{F}_b\left(k\right)]}, \tag{B35}$$

for the generalized polarization densities and

$$\Phi\left(\boldsymbol{r}\right) = -\frac{I}{\sigma^{\rm c}}\int dk\frac{e^{ikx}}{2\pi k}\frac{\sinh\left(ky\right)}{\cosh\left(kW/2\right)[1+\sum_b\Theta_b^2\mathcal{F}_b\left(k\right)]}. \tag{B36}$$

for the electrostatic potential.

Appendix C: Nonlocal Resistance

In this section, we compute the nonlocal resistance (NLR) in the absence of magnetic field, which is defined as

$$R_{nl}\left(x\right) = \frac{1}{I}[\Phi\left(x,-w/2\right)-\Phi\left(x,+w/2\right)]. \tag{C1}$$

Substituting the electrostatic potential (B36) into (C1), we obtain the following integral form for the NLR:

$$\frac{R_{nl}(x)}{R_{\rm xx}} = \frac{1}{\pi}\int_{-\infty}^{\infty}dk\frac{e^{ikx}}{k}\frac{\tanh\left(kw/2\right)}{1+\sum_b\Theta_b^2\mathcal{F}_b\left(k\right)}, \tag{C2}$$

with $R_{\rm xx}=1/\sigma^c$. The above result for the NLR can be expanded as follows

$$\frac{R_{nl}(x)}{R_{\rm xx}} = \sum_{n=0}^{\infty}\mathcal{R}^n\left(x\right), \tag{C3}$$

$$\mathcal{R}^n\left(x\right) = \sum_{\boldsymbol{a}^n}\mathcal{R}_{\boldsymbol{a}^n}\left(x\right), \tag{C4}$$

with $\boldsymbol{a}^n=(a_1,a_2,\cdots,a_n)$. The expression for $\mathcal{R}_{\boldsymbol{a}^n}\left(x\right)$ is given by:

$$\mathcal{R}_{\boldsymbol{a}^n}(x) = \frac{1}{\pi}\left(-1\right)^n\int_{-\infty}^{+\infty}\frac{dk\,e^{ikx}}{k\coth\left(kw/2\right)}\prod_{\imath=1}^{n}\Theta_{a_\imath}^2\mathcal{F}_{a_\imath}\left(k\right). \tag{C5}$$

Next, we obtain asymptotic expressions for the various terms in the above expansion. For $n=0$, $\mathcal{R}^0\left(x\right)$ reduces to the Ohmic NLR:

$$\mathcal{R}^0(x) = \frac{2}{\pi}\ln\left|\coth\left(\frac{\pi x}{2w}\right)\right|. \tag{C6}$$

Explicitly, it is van der Paw resistance, which behaves as $\mathcal{R}_{\rm vdP}\simeq\frac{4}{\pi}e^{-|x|/\mathcal{L}_0}$ for $|x|\gg w$ where $\mathcal{L}_0=w/\pi$. At large $|x|$, and for $w\ll\ell_\nu$, the $n=1$ term is $\mathcal{R}^1=\sum_a\mathcal{R}_a^1$, where

$$\mathcal{R}_a^1\left(x\right)\simeq\Theta_a^2\frac{w}{2\mathcal{L}_a}e^{-|x|/\mathcal{L}_a}. \tag{C7}$$

In earlier work[27], we showed that a modest nonuniform strain can result in rather large valley Hall angles $\theta_v\sim 1$. Thus, in order to accurately describe the NLR we need to consider high order terms in the expansion, i.e. those with $n>1$. But we here just pick out terms $\mathcal{R}_{\boldsymbol{a}^n}$ with same eigenmode $a_\imath=a$ i.e., $R_{nl}/R_{\rm xx}\simeq\mathcal{R}^0+\sum_a\mathcal{R}^a$, being

$$\begin{aligned}\mathcal{R}^a(x) &= \int_{-\infty}^{+\infty}\frac{dk}{\pi k}\frac{e^{ikx}}{\coth\left(kw/2\right)}\sum_{n=1}^{\infty}\left(-1\right)^n\left[\Theta_a^2\mathcal{F}_a\left(k\right)\right]^n\\ &= \frac{\Theta_a^2}{1+\Theta_a^2}\frac{W}{2\mathcal{L}_a^r}e^{-|x|/\mathcal{L}_a^r},\end{aligned} \tag{C8}$$

where $\mathcal{L}_a^r=\sqrt{1+\Theta_a^2}\mathcal{L}_a$ is renormalized decay lengths of each eigenmode[27]. Finally, we obtain total NLR $R_{nl}/R_{\rm xx}=\mathcal{R}^0+\delta\mathcal{R}_{nl}$

$$\frac{R_{nl}(x)}{R_{\rm xx}} \simeq \overbrace{\frac{4}{\pi}e^{-|x|/\mathcal{L}_0}}^{\mathcal{R}^0} + \overbrace{\sum_a\underbrace{\frac{\Theta_a^2}{1+\Theta_a^2}\frac{w}{2\mathcal{L}_a^r}e^{-|X|/\mathcal{L}_a^r}}_{\mathcal{R}^a}}^{\delta\mathcal{R}_{nl}}, \tag{C9}$$

The first term is the Ohmic contribution, $\mathcal{R}^0$, and the second term contains the sum of the exponentially decaying contributions for each eigenmode, $\mathcal{R}^a$. Near the current injection point ($|x| \lesssim \mathcal{L}_0$), R_{nl} is dominated by the ohmic contribution, $\mathcal{R}^0$, which will become negligible at sufficiently large distances (i.e. for $|x| \gg \mathcal{L}_0$).

Here we focus on the behavior of R_{nl}, when contribution of the eigenmodes of the diffusion equation dominate over the Ohmic contribution, i.e. when $\delta\mathcal{R}_{nl} \gg \mathcal{R}^0$.

Appendix D: Suppression of the Hanle oscillation

In this section, we provide the details of the derivation and solution of the diffusion equations in the presence of an in-plane magnetic field. Note that the Larmor frequency $\omega_L \ll \mu_F$, where μ_F is the Fermi level. The in-plane magnetic field, which we shall take parallel to the direction of the electric field applied to the device, induces precession of the spin-degree of freedom, whilst the valley is not affected. This mixes the out-of-plane spin component along z with the spin in-plane components along the x and y axes. Thus, our ansatz for the density-matrix distribution function in the QBE must be now expanded in terms of γ_ν matrices taken from the larger set $\{\hat{s}_o\hat{\tau}_o, \hat{s}_o\hat{\tau}_z, \hat{s}_x\hat{\tau}_o, \hat{s}_y\hat{\tau}_o, \hat{s}_z\hat{\tau}_o, \hat{s}_x\hat{\tau}_z, \hat{s}_y\hat{\tau}_z, \hat{s}_z\hat{\tau}_z\}$.

In order to simplify the calculations described below, the deviation of the distribution function from equilibrium, i.e. $\delta n_{\boldsymbol{k}} = n_{\boldsymbol{k}} - n^0_{\boldsymbol{k}}$, will be slit into two parts, $\delta n_{\boldsymbol{k}} = \delta n^+_{\boldsymbol{k}} + \delta n^-_{\boldsymbol{k}}$, with

$$\delta n^+_{\boldsymbol{k}} \simeq \sum_{\mathrm{i}} \gamma_{\mathrm{i}} \left[\mu^{\mathrm{i}}(\boldsymbol{r}) + \boldsymbol{v}^{\mathrm{i}}(\boldsymbol{r}) \cdot \hbar\boldsymbol{k}\right] \left[-\partial_\epsilon n^0(\epsilon)\right]_{\epsilon=\mu_F}, \tag{D1}$$

$$\delta n^-_{\boldsymbol{k}} \simeq \sum_{\mathrm{j}} \gamma_{\mathrm{j}} \left[\mu^{\mathrm{j}}(\boldsymbol{r}) + \boldsymbol{v}^{\mathrm{j}}(\boldsymbol{r}) \cdot \hbar\boldsymbol{k}\right] \left[-\partial_\epsilon n^0(\epsilon)\right]_{\epsilon=\mu_F}, \tag{D2}$$

where $\mathrm{i} \in \{c, sv, v, s\}$ and $\mathrm{j} \in \{xo, yo, xz, yz\}$.

The form of the collision integral (A18) is determined by the ansatz for density matrix $\delta n_{\boldsymbol{k}}$, which in turn follows from the forms of the T-matrix ($\propto \{\hat{s}_o, \hat{s}_z\}$), the pseudo-magnetic field arising from nonuniform strain ($\propto \{\hat{\tau}_o, \hat{\tau}_z\}$), and the (Zeeman) magnetic field ($\{\hat{s}_o, \hat{s}_y\}$). To compute the collision integral, it is convenient to also split the T-matrix into two parts, i.e., $T_{\boldsymbol{kp}} = T^o_{\boldsymbol{kp}} + T^z_{\boldsymbol{kp}}$, with

$$T^o_{\boldsymbol{kp}} = t_c \mathbb{1} \cos\left(\frac{\theta}{2}\right), \tag{D3}$$

$$T^z_{\boldsymbol{kp}} = i t_s \hat{s}_z \sin\left(\frac{\theta}{2}\right), \tag{D4}$$

which obey:

$$\left[\delta n^-_{\boldsymbol{k}}, T^z_{\boldsymbol{kp}}\right]_+ = 0, \tag{D5}$$

$$\left[\delta n^-_{\boldsymbol{k}}, T^o_{\boldsymbol{kp}}\right]_- = 0, \tag{D6}$$

$$\left[\delta n^+_{\boldsymbol{k}}, T_{\boldsymbol{kp}}\right]_- = 0, \tag{D7}$$

where $[A, B]_\pm = AB \pm BA$. Next, using the above ansatz, the collision integral (A18) reduces to:

$$\begin{aligned}\mathcal{I}[\delta n_{\boldsymbol{k}}] = {} & \frac{\pi}{\hbar} n_{\mathrm{i}} \sum_{\boldsymbol{p}} \delta[\epsilon(p) - \epsilon(q)]\, 2\hat{T}_{\boldsymbol{kp}} \hat{T}^*_{\boldsymbol{kp}} (\delta n^+_{\boldsymbol{p}} - \delta n^+_{\boldsymbol{k}}) \\ & + \frac{\pi}{\hbar} n_{\mathrm{i}} \sum_{\boldsymbol{p}} \delta[\epsilon(p) - \epsilon(q)]\, 2\hat{T}_{\boldsymbol{kp}} \hat{T}^{o*}_{\boldsymbol{kp}} (\delta n^-_{\boldsymbol{p}} - \delta n^-_{\boldsymbol{k}}) \\ & - \frac{\pi}{\hbar} n_{\mathrm{i}} \sum_{\boldsymbol{p}} \delta[\epsilon(p) - \epsilon(q)]\, 2\hat{T}_{\boldsymbol{kp}} \hat{T}^{z*}_{\boldsymbol{kp}} (\delta n^-_{\boldsymbol{p}} + \delta n^-_{\boldsymbol{k}}).\end{aligned} \tag{D8}$$

Hence,

$$\begin{aligned}2\hat{T}^+_{\boldsymbol{kp}} \hat{T}^*_{\boldsymbol{kp}} = {} & \left[|t_c|^2 (1 + \cos\theta) + |t_s|^2 (1 - \cos\theta)\right] \gamma^c \\ & + 2\mathrm{Im}(t_c t_s^*) \sin\theta \gamma^s\end{aligned} \tag{D9}$$

$$2\hat{T}_{\boldsymbol{kp}} \hat{T}^{o*}_{\boldsymbol{kp}} = |t_c|^2 (1 + \cos\theta) \gamma^c + i t_s t_c^* \sin\theta \gamma^s, \tag{D10}$$

$$2\hat{T}_{\boldsymbol{kp}} \hat{T}^{z*}_{\boldsymbol{kp}} = |t_s|^2 (1 - \cos\theta) \gamma^c - i t_c t_s^* \sin\theta \gamma^s, \tag{D11}$$

In addition, we need to compute the differences and sums:

$$\delta n^-_{\boldsymbol{p}} - \delta n^-_{\boldsymbol{k}} = \left[-\partial_\epsilon n^0(\epsilon)\right]_{\epsilon=\mu_F} \sum_{\mathrm{j}} \gamma_{\mathrm{j}} \boldsymbol{v}_{\mathrm{j}}(\boldsymbol{r}) \cdot \hbar(\boldsymbol{p} - \boldsymbol{k}), \tag{D12}$$

$$\delta n^+_{\boldsymbol{p}} - \delta n^+_{\boldsymbol{k}} = \left[-\partial_\epsilon n^0(\epsilon)\right]_{\epsilon=\mu_F} \sum_{\mathrm{i}} \gamma_{\mathrm{i}} \boldsymbol{v}_{\mathrm{i}}(\boldsymbol{r}) \cdot \hbar(\boldsymbol{p} - \boldsymbol{k}), \tag{D13}$$

$$\begin{aligned}\delta n^-_{\boldsymbol{p}} + \delta n^-_{\boldsymbol{k}} = {} & \left[-\partial_\epsilon n^0(\epsilon)\right]_{\epsilon=\mu_F} \sum_{\mathrm{j}} \gamma_{\mathrm{j}} \boldsymbol{v}_{\mathrm{j}}(\boldsymbol{r}) \cdot \hbar(\boldsymbol{p} + \boldsymbol{k}) \\ & + \left[-\partial_\epsilon n^0(\epsilon)\right]_{\epsilon=\mu_F} \sum_{\mathrm{j}} 2\gamma_{\mathrm{j}} \mu_{\mathrm{j}}(\boldsymbol{r}).\end{aligned} \tag{D14}$$

Substituting Eqs. (D9)-(D14) into the collision integral (D8), the explicit form of the collision integral is split into three contributions: $\mathcal{I}[\delta n_{\boldsymbol{k}}] = \mathcal{I}^+[\delta n_{\boldsymbol{k}}] + \mathcal{I}^0[\delta n_{\boldsymbol{k}}] + \mathcal{I}^-[\delta n_{\boldsymbol{k}}]$, with

$$\begin{aligned}\mathcal{I}^+[\delta n_{\boldsymbol{k}}] = {} & \left[\partial_\epsilon n^0(\epsilon)\right]_{\epsilon=\mu_F} \hbar\boldsymbol{k} \cdot \left\{\frac{\gamma^c}{\tau} \sum_{\mathrm{i}} \gamma^{\mathrm{i}} \boldsymbol{v}_{\mathrm{i}}(\boldsymbol{r}) \right. \\ & \left. + \gamma^s \omega_s \sum_{\mathrm{i}} \gamma^{\mathrm{i}} \boldsymbol{v}_{\mathrm{i}}(\boldsymbol{r}) \times \hat{\boldsymbol{z}}\right\},\end{aligned} \tag{D15}$$

$$\mathcal{I}^0[\delta n_{\boldsymbol{k}}] = \left[\partial_\epsilon n^0(\epsilon)\right]_{\epsilon=\mu_F} \frac{\gamma^c}{\tau_{s,xy}} \sum_{\mathrm{j}} \gamma^{\mathrm{j}} \mu_{\mathrm{j}}(\boldsymbol{r}), \tag{D16}$$

$$\begin{aligned}\mathcal{I}^-[\delta n_{\boldsymbol{k}}] = {} & \left[\partial_\epsilon n^0(\epsilon)\right]_{\epsilon=\mu_F} \hbar\boldsymbol{k} \cdot \left\{\frac{\gamma^c}{\tilde{\tau}} \sum_{\mathrm{j}} \gamma^{\mathrm{j}} \boldsymbol{v}_{\mathrm{j}}(\boldsymbol{r}) \right. \\ & \left. + i\gamma^s \omega_s \sum_{\mathrm{j}} \gamma^{\mathrm{j}} \boldsymbol{v}_{\mathrm{j}}(\boldsymbol{r}) \times \hat{\boldsymbol{z}}\right\},\end{aligned} \tag{D17}$$

where i $= (c, sv, v, s)$, j $= (xo, yo, xz, yz)$ and we define other two kinds of relaxation times to describe the collision of electrons:

$$\frac{1}{\tau_{s,xy}(k)} = \frac{kn_{\rm i}}{4\hbar^2 v_F}\left[4\left|t_s(k)\right|^2\right], \tag{D18}$$

$$\frac{1}{\tilde{\tau}(k)} = \frac{kn_{\rm i}}{4\hbar^2 v_F}\left[\left|t_c(k)\right|^2 + \left|t_s(k)\right|^2\right], \tag{D19}$$

Notice that, in the presence of an in-plane magnetic field the term $\mathcal{I}^0\left[\delta n_{\boldsymbol{k}}\right]$ in the colission integral introduces an additional relaxation time, $\tau_{s,xy}(k)$.

In addition to spin (spin-valley) current, the in-plane magnetic field couples the out-of-plane and in-plane components of the spin current, $\boldsymbol{J}^{xo}$ and $\boldsymbol{J}^{yo}$ (spin-valley currents, $\boldsymbol{J}^{xz}$ and $\boldsymbol{J}^{yz}$). Here we take the magnetic field to be parallel to the applied electric field, i.e. $\boldsymbol{H} \parallel \hat{\boldsymbol{y}}$, and thus the following generalized density N and current $\boldsymbol{J}$ appear in our diffusion equations:

$$\boldsymbol{J} = \begin{bmatrix}\boldsymbol{J}_{\parallel}\\ \boldsymbol{J}_{\perp}\end{bmatrix}, \boldsymbol{J}_{\parallel} = \begin{bmatrix}\boldsymbol{J}^{c}\\ \boldsymbol{J}^{sv}\\ \boldsymbol{J}^{xz}\\ \boldsymbol{J}^{yo}\end{bmatrix}, \boldsymbol{J}_{\perp} = \begin{bmatrix}\boldsymbol{J}^{v}\\ \boldsymbol{J}^{s}\\ \boldsymbol{J}^{xo}\\ \boldsymbol{J}^{yz}\end{bmatrix}, \tag{D20}$$

$$N = \begin{bmatrix}N_{\parallel}\\ N_{\perp}\end{bmatrix}, N_{\parallel} = \begin{bmatrix}N^{c}\\ N^{sv}\\ N^{xz}\\ N^{yo}\end{bmatrix}, N_{\perp} = \begin{bmatrix}N^{v}\\ N^{s}\\ N^{xo}\\ N^{yz}\end{bmatrix}, \tag{D21}$$

where we have divided the longitudinal and transverse modes. Let us first focus on the continuity equations. In the steady state, they read:

$$\partial_i J_i^{\mu} = -(\tau_{sr}^{-1})_{\nu}^{\mu} N^{\nu} + \omega_{\nu}^{\mu} N^{\nu}, \tag{D22}$$

which is obtained by tracing the linearized QBE, i.e. taking $\frac{g_s g_v}{4}\sum_{\boldsymbol{k}} e\mathrm{Tr}\left[\gamma^{\mu}\left(\mathrm{QBE}\right)\right]$. In the above expression

$$\tau_{sr}^{-1} = \begin{bmatrix}\tau_0^{-1} & 0\\ 0 & \tau_0^{-1}\end{bmatrix}, \tau_0^{-1} = \begin{bmatrix}0 & 0 & 0 & 0\\ 0 & 0 & 0 & 0\\ 0 & 0 & \tau_{s,xy}^{-1} & 0\\ 0 & 0 & 0 & \tau_{s,xy}^{-1}\end{bmatrix}, \tag{D23}$$

$$\omega = \begin{bmatrix}\omega_0 & 0\\ 0 & \omega_0\end{bmatrix}, \omega_0 = \begin{bmatrix}0 & 0 & 0 & 0\\ 0 & 0 & +\omega_L & 0\\ 0 & -\omega_L & 0 & 0\\ 0 & 0 & 0 & 0\end{bmatrix}. \tag{D24}$$

The matrix τ_{sr}^{-1} describes the spin relaxation for spin polarized in the x-y plane. In our microscopic model, s_z is a good quantum number and there is no relaxation. The second term describes the spin precession induced by an in-plane magnetic field in y-axis direction. We parameterize the strength of the in-plane magnetic field H by the Larmor frequency $\omega_L = g\mu_B H/\hbar$.

The constitutive relations for the generalized currents, J_i^{μ} is given by following equations:

$$\mathcal{D}\partial_i N^{\mu} - \sigma_D E_i^{\mu} = \left[-\delta_{\nu}^{\mu}\delta_{ij} + \tau\omega_{\nu}^{\mu}\delta_{ij} + (R_H)_{\nu}^{\mu}\epsilon_{ij}\right] J_j^{\nu}, \tag{D25}$$

where

$$R_H = \begin{bmatrix}0 & R_H^0\\ R_H^0 & 0\end{bmatrix}, R_H^0 = \begin{bmatrix}\omega_v\tau & \omega_s\tau & 0 & 0\\ \omega_s\tau & \omega_v\tau & 0 & 0\\ 0 & 0 & \omega_v\tau & \omega_s\tau\\ 0 & 0 & \omega_s\tau & \omega_v\tau\end{bmatrix}. \tag{D26}$$

For the sake of simplicity, we have assumed that the relaxation rates for all currents are the same and equal to Drude relaxation time ($\tilde{\tau} \simeq \tau$) (See expressions for $\tilde{\tau}$ in Eq. (D19) for $i = (xo, yo, xz, yz)$ and τ in Eq. (A24) for $i = (c, sv, v, s)$. Thus, we take $\mathcal{D} = v_F^2\tau/2$ ($\sigma_D = ne^2\tau/m$) to be the same for all types of currents. These assumptions can be relaxed, and will not alter our conclusions qualitatively. R_H is the coupling matrix that couples the different currents with each other due to the local impurities and the strain pseudo-magnetic field.

Solving the constitutive equations (D25) for the currents J_i^{μ} we obtain:

$$J_i^{\mu} = -(D_{ij})_{\nu}^{\mu}\partial_j N^{\nu} + (\sigma_{ij})_{\nu}^{\mu} E_j^{\nu}. \tag{D27}$$

As pointed out in the main text, the diffusion matrix is a rank-2 tensor in the space indices $i, j = x, y$, and therefore it can be split into a symmetric ($\propto \delta_{ij}$) and antisymmetric ($\propto \epsilon_{ij}$) parts according to $D_{ij} = D_0\delta_{ij} + D_H\epsilon_{ij}$ where

$$D_0 = \begin{bmatrix}D_0^0 & 0\\ 0 & D_0^0\end{bmatrix}, D_0^0 = \mathcal{D}_r\begin{bmatrix}\eta_c & \eta_{sv} & \eta_{xz} & \eta_{yo}\\ \eta_{sv} & \eta_c & \eta_{yo} & \eta_{xz}\\ \eta_{xz} & \eta_{yo} & \eta_c & \eta_{sv}\\ \eta_{yo} & \eta_{xz} & \eta_{sv} & \eta_c\end{bmatrix}, \tag{D28}$$

$$D_H = \begin{bmatrix}0 & D_H^0\\ D_H^0 & 0\end{bmatrix}, D_H^0 = \mathcal{D}_r\begin{bmatrix}\theta_v & \theta_s & \theta_{xo} & \theta_{yz}\\ \theta_s & \theta_v & \theta_{yz} & \theta_{xo}\\ \theta_{xo} & \theta_{yz} & \theta_v & \theta_s\\ \theta_{yz} & \theta_{xo} & \theta_s & \theta_v\end{bmatrix}. \tag{D29}$$

$\mathcal{D}_r, \eta_{\mu}, \theta_{\mu}$ are rather complicated functions of $\omega_v\tau, \omega_s\tau$ and $\omega_L\tau$, and are not given here. Similarly, the conductivity matrix can be obtained by replacing the diffusion constant $\mathcal{D}$ with the Drude conductivity σ_D.

In the presence of an in-plane magnetic field, the system response consists of eight types of currents. Recall that the magnetic field acts only as a Zeeman term that induces precession, and does not introduce a Lorentz force (i.e. $\boldsymbol{F}_{\boldsymbol{k}}^{B} = 0$ in Eq. (A9), as mentioned above). Accounting (phenomenologically) for spin relaxation, the constitutive and continuity equations in the presence of the magnetic field read:

$$J_i^{\mu} = -(D_{ij})_{\nu}^{\mu}\partial_j N^{\nu} + (\sigma_{ij})_{\nu}^{\mu} E_j^{\nu}, \tag{D30}$$

$$\partial_i J_i^{\mu} = -\frac{\delta_{\nu}^{\mu}}{\tau^{\nu}} N^{\nu} + \omega_{\nu}^{\mu} N^{\nu}, \tag{D31}$$

where

$$D_0 = \begin{bmatrix}D_0^0 & 0\\ 0 & D_0^0\end{bmatrix}, D_0^0 = \mathcal{D}_r\begin{bmatrix}1 & \eta & 0 & 0\\ \eta & 1 & 0 & 0\\ 0 & 0 & 1 & \eta\\ 0 & 0 & \eta & 1\end{bmatrix}, \tag{D32}$$

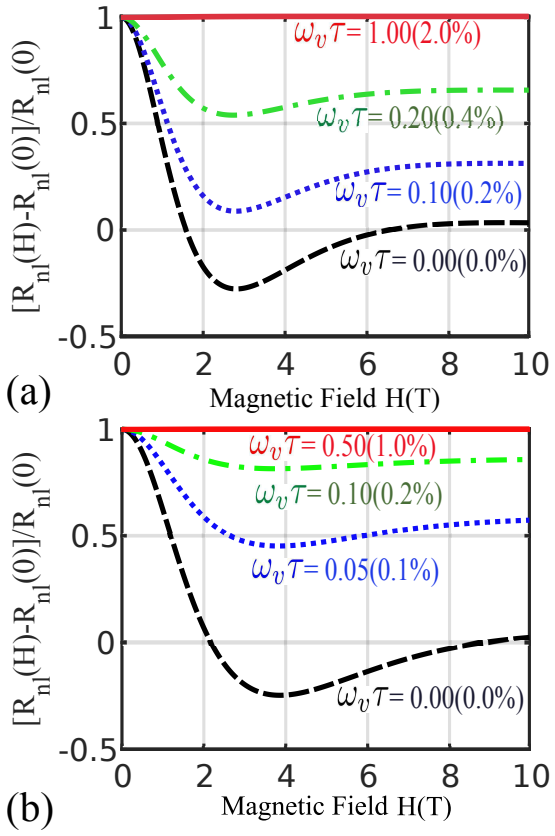

FIG. 3. (Color online) Nonlocal resistance $R_{nl}(H)$, in the unit of $R_{nl}(0)$, are plotted against magnetic field H for different chemical potential (a) $\mu_F = 0.15$ eV and (b) $\mu_F = -0.10$ eV. Drude conductivity σ_D, Drude relaxation time τ and the scattering rate of spin, $\omega_s\tau$, can be obtained from the parameters of a microscopic scattering model[53] : impurity density $n_{\rm imp} = 5.0 \times 10^{10} cm^{-2}$, scalar potential $\mathcal{V}_D = 50$ meV, SOC potential [33] $\mathcal{V}_S = 5$ meV, defect size $R = 20$ nm, and associated momentum cutoff $k_c = 2/R$. On the other hand, fairly modest strain can sustain a large valley Hall effect[27], $\omega_v\tau(\gtrsim 1)$. $\omega_v\tau = 1$ can be induced by applying along the y direction an average (uniaxial) strain of 2%. Parameters: $\ell_s = 0.53\mu$m, $\ell_v = 0.53\mu$m, $w = 0.50\mu$m, $x = 2.00\mu$m and $y = 0.25\mu$m.

$$D_H = \begin{bmatrix} 0 & D_H^0 \\ D_H^0 & 0 \end{bmatrix}, D_H^0 = \mathcal{D}_r \begin{bmatrix} \theta_v & \theta_s & 0 & 0 \\ \theta_s & \theta_v & 0 & 0 \\ 0 & 0 & \theta_v & \theta_s \\ 0 & 0 & \theta_s & \theta_v \end{bmatrix}. \quad \text{(D33)}$$

Substituting continuity equations (D31) into the divergence of constitutive equations (D30), the diffusion equations away from the boundaries take again a form similar to Eq. (B17),

$$\partial_i^2 N^\mu - \mathcal{M}_\nu^\mu N^\nu = 0. \quad \text{(D34)}$$

However, this time the diffusion matrix is 4×4 in order to accommodate the additional response modes introduced by the precession term:

$$\mathcal{M} \simeq \begin{bmatrix} \ell_v^{-2} & -\eta\ell_s^{-2} & +\eta\ell_L^{-2} & 0 \\ -\eta\ell_v^{-2} & \ell_s^{-2} & -\ell_L^{-2} & 0 \\ 0 & +\ell_L^{-2} & \ell_s^{-2} & -\eta\ell_v^{-2} \\ 0 & -\eta\ell_L^{-2} & -\eta\ell_s^{-2} & \ell_v^{-2} \end{bmatrix}. \quad \text{(D35)}$$

The eigenvalues of the above diffusion matrix are

$$E_\pm^\eta = \frac{\ell_v^{-2} + \ell_s^{-2} \mp i\ell_L^{-2}}{2} + \frac{\eta}{2}\sqrt{\Delta_\pm}. \quad \text{(D36)}$$

with

$$\Delta_\pm = \left(\ell_v^{-2} - \ell_s^{-2} \pm i\ell_L^{-2}\right)^2 + 4\eta_{zz}^2\ell_v^{-2}\left(\ell_s^{-2} \mp i\ell_L^{-2}\right). \quad \text{(D37)}$$

Hence, following the same procedure to find the solution as in the case with $H = 0$, we arrive at the following result for the NLR:

$$\frac{R_{nl}(x,H)}{R_{\rm xx}} = \frac{1}{\pi}\int_{-\infty}^{\infty} dk \frac{e^{ikx}}{k} \frac{\tanh(kw/2)}{1 + \sum_b \Theta_b^2 \mathcal{F}_b(k)}, \quad \text{(D38)}$$

where we sum over four transverse eigenmodes $\{v, s, xo, yz\}$ in the denominator of the above integral. The above equation is the basis of the analysis about the suppression of the Hanle effect described in the main text.

Fig. 3 shows the NLR, $R_{nl}(x,H)$ normalized to its value at zero in-plane magnetic field, $R_{nl}(x,H=0)$ versus H, for different chemical potentials [(a) $\mu_F = 0.15$ eV and (b) $\mu_F = -0.10$ eV]. As noticed in the main text, by setting $\omega_v\tau = 0$, the result of Abanin *el al.*[41] is recovered. In this case, the diffusion lengths of the (spin) eigenmodes, $\ell_{s\pm} = (\ell_s^{-2} \pm i\ell_L^{-2})^{-1/2}$ become complex (with imaginary part $\ell_L^{-2} \propto H$), which leads to the development of an oscillatory component in the NLR (Hanle oscillation). Upon increasing the amount of nonuniform strain, we find that the oscillating part of the NLR is suppressed and even disappears for strains of the order of $\sim 1\%$. This shows that our result concerning the suppression of the Hanle oscillation for nonuniform strain of the order of a few percents maximum is robust against the change of the carrier density and sign.

[1] D. Xiao, M.-C. Chang, and Q. Niu, Reviews of modern physics **82**, 1959 (2010).
[2] J. Sinova, S. O. Valenzuela, J. Wunderlich, C. H. Back, and T. Jungwirth, Rev. Mod. Phys. **87**, 1213 (2015).
[3] N. Nagaosa, J. Sinova, S. Onoda, A. H. MacDonald, and N. P. Ong, Rev. Mod. Phys. **82**, 1539 (2010).
[4] J. Sinova, D. Culcer, Q. Niu, N. Sinitsyn, T. Jungwirth, and A. MacDonald, Phys. Rev. Lett. **92**, 126603 (2004).

[5] D. Huertas-Hernando, F. Guinea, and A. Brataas, Phys. Rev. B **74**, 155426 (2006).
[6] X. Xu, W. Yao, D. Xiao, and T. F. Heinz, Nature Physics **10**, 343 (2014).
[7] T. Cao, G. Wang, W. Han, H. Ye, C. Zhu, J. Shi, Q. Niu, P. Tan, E. Wang, B. Liu, *et al.*, Nature communications **3**, 887 (2012).
[8] A. Rycerz, J. Tworzydło, and C. Beenakker, Nature Physics **3**, 172 (2007).
[9] E. J. Sie, J. W. McIver, *et al.*, Nature Materials **14**, 290 (2015).
[10] Z. Zhu, Y. Cheng, and U. Schwingenschlögl, Physical Review B **84**, 153402 (2011).
[11] Y. Zhang, T.-R. Chang, B. Zhou, Y.-T. Cui, H. Yan, Z. Liu, F. Schmitt, J. Lee, R. Moore, Y. Chen, *et al.*, Nature nanotechnology **9**, 111 (2014).
[12] A. C. Neto and F. Guinea, Phys. Rev. Lett. **103**, 026804 (2009).
[13] M. Gmitra, D. Kochan, and J. Fabian, Physical review letters **110**, 246602 (2013).
[14] S. Irmer, T. Frank, S. Putz, M. Gmitra, D. Kochan, and J. Fabian, Physical Review B **91**, 115141 (2015).
[15] J. Ding, Z. Qiao, W. Feng, Y. Yao, and Q. Niu, Physical Review B **84**, 195444 (2011).
[16] M. Gmitra and J. Fabian, Physical Review B **92**, 155403 (2015).
[17] Z. Wang, D.-K. Ki, H. Chen, H. Berger, A. H. MacDonald, and A. F. Morpurgo, Nature communications **6**, 8339 (2015).
[18] A. W. Cummings, J. H. Garcia, J. Fabian, and S. Roche, Physical review letters **119**, 206601 (2017).
[19] J. H. Garcia, A. W. Cummings, and S. Roche, Nano letters **17**, 5078 (2017).
[20] M. I. Katsnelson, *Graphene: carbon in two dimensions* (Cambridge University Press, 2012).
[21] A. H. Castro Neto, F. Guinea, N. Peres, K. S. Novoselov, and A. K. Geim, Rev. Mod. Phys. **81**, 109 (2009).
[22] C. E. Nebel, Nature materials **12**, 690 (2013).
[23] J. R. Schaibley, H. Yu, G. Clark, P. Rivera, J. S. Ross, K. L. Seyler, W. Yao, and X. Xu, Nature Reviews Materials **1**, 16055 (2016).
[24] D. Xiao, W. Yao, and Q. Niu, Physical Review Letters **99**, 236809 (2007).
[25] R. Gorbachev, J. Song, Y. GL, A. Kretinin, F. Withers, Y. Cao, Y. Mishchenko, I. Grigorieva, K. Novoselov, L. Levitov, and A. Geim, Science **346**, 448 (2014).
[26] M. Beconcini, F. Taddei, and M. Polini, Physical Review B **94**, 121408 (2016).
[27] X.-P. Zhang, C. Huang, and M. A. Cazalilla, 2D Mater. **4**, 024007 (2017).
[28] Y. Shimazaki, M. Yamamoto, I. V. Borzenets, K. Watanabe, T. Taniguchi, and S. Tarucha, Nature Physics **11**, 1032 (2015).
[29] K. F. Mak, K. L. McGill, J. Park, and P. L. McEuen, Science **344**, 1489 (2014).
[30] J. Lee, K. F. Mak, and J. Shan, Nature nanotechnology **11**, 421 (2016).
[31] H. Zeng, J. Dai, W. Yao, D. Xiao, and X. Cui, Nature nanotechnology **7**, 490 (2012).
[32] J. Lee, Z. Wang, H. Xie, K. F. Mak, and J. Shan, Nature materials **16**, 887 (2017).
[33] J. Balakrishnan, G. K. W. Koon, A. Avsar, Y. Ho, J. H. Lee, M. Jaiswal, S.-J. Baeck, J.-H. Ahn, A. Ferreira, M. A. Cazalilla, and A. H. Castro Neto, Nature Communications **5**, 4748 (2014).
[34] J. Balakrishnan, G. K. W. Koon, M. Jaiswal, A. H. C. Neto, and B. Özyilmaz, Nature Physics **9**, 284 (2013).
[35] C. Weeks, J. Hu, J. Alicea, M. Franz, and R. Wu, Physical Review X **1**, 021001 (2011).
[36] D. Ma, Z. Li, and Z. Yang, Carbon **50**, 297 (2012).
[37] A. Avsar, J. Y. Tan, T. Taychatanapat, J. Balakrishnan, G. Koon, Y. Yeo, J. Lahiri, A. Carvalho, A. Rodin, E. O?Farrell, *et al.*, Nature communications **5**, 4875 (2014).
[38] C. Safeer, J. Ingla-Aynés, F. Herling, J. H. Garcia, M. Vila, N. Ontoso, M. R. Calvo, S. Roche, L. E. Hueso, and F. Casanova, arXiv preprint arXiv:1810.12481 (2018).
[39] L. A. Benítez, J. F. Sierra, W. S. Torres, A. Arrighi, F. Bonell, M. V. Costache, and S. O. Valenzuela, Nature Physics **14**, 303 (2018).
[40] C. Huang, Y. D. Chong, and M. A. Cazalilla, Phys. Rev. Lett. **119**, 136804 (2017).
[41] D. A. Abanin, A. V. Shytov, L. S. Levitov, and B. I. Halperin, Phys. Rev. B **79**, 035304 (2009).
[42] T. Völkl, D. Kochan, T. Ebnet, S. Ringer, D. Schiermeier, P. Nagler, T. Korn, C. Schüller, J. Fabian, D. Weiss, *et al.*, arXiv preprint arXiv:1809.10475 (2018).
[43] A. A. Kaverzin and B. J. van Wees, Phys. Rev. B **91**, 165412 (2015).
[44] Y. Wang, X. Cai, J. Reutt-Robey, *et al.*, Phys. Rev. B **92**, 161411 (2015).
[45] J. C. Song and G. Vignale, arXiv preprint arXiv:1805.05955 (2018).
[46] F. Guinea, M. Katsnelson, and A. Geim, Nat. Phys. **6**, 30 (2010).
[47] M. A. Vozmediano, M. Katsnelson, and F. Guinea, Physics Reports **496**, 109 (2010).
[48] B. Amorim, A. Cortijo, F. De Juan, A. Grushin, F. Guinea, A. Gutiérrez-Rubio, H. Ochoa, V. Parente, R. Roldán, P. San-Jose, *et al.*, Physics Reports **617**, 1 (2016).
[49] M. A. Cazalilla, H. Ochoa, and F. Guinea, Phys. Rev. Lett. **113**, 077201 (2014).
[50] A. Avsar, J. H. Lee, G. K. W. Koon, and B. Özyilmaz, 2D Materials **2**, 044009 (2015).
[51] I. D'Amico and G. Vignale, Physical Review B **65**, 085109 (2002).
[52] S.-Q. Shen, Physical review letters **95**, 187203 (2005).
[53] C. Huang, Y. D. Chong, G. Vignale, and M. A. Cazalilla, Phys. Rev. B **93**, 165429 (2016).
[54] T. Ando, Journal of the Physical Society of Japan **84**, 114705 (2015).
[55] H. Ishizuka and N. Nagaosa, Phys. Rev. B **96**, 165202 (2017).
[56] R. Raimondi, P. Schwab, C. Gorini, and G. Vignale, Annalen der Physik **524**, n/a (2012).
[57] In the present treatment, the spin and valley relaxation times are introduced phenomenologically. However, it should be noticed that they can be derived from a microscopic model, see e.g. Refs.[27,53]. In particular, the valley relaxation accounts for the inter-valley scattering that arises from short-range scatterers. As we have shown in Ref.[27], the inter-valley scattering induced by a dilute concentration of the latter is not detrimental to the generation of valley currents due to nonuniform strain. Higher concentrations of short range scatterers may quickly deteriorate the mobility in the device and eventually lead to Anderson localization.
[58] A. Ferreira, T. G. Rappoport, M. A. Cazalilla, and A. C.

Neto, Physical review letters **112**, 066601 (2014).
[59] H.-Y. Yang, C. Huang, H. Ochoa, and M. A. Cazalilla, Physical Review B **93**, 085418 (2016).
[60] R. Suzuki, M. Sakano, Y. Zhang, R. Akashi, D. Morikawa, A. Harasawa, K. Yaji, K. Kuroda, K. Miyamoto, T. Okuda, *et al.*, Nature nanotechnology **9**, 611 (2014).
[61] C. Huang, M. Milletarì, and M. A. Cazalilla, Physical Review B **96**, 205305 (2017).
[62] D. M. Basko, Physical Review B **78**, 115432 (2008).
[63] C. Huang, Y. D. Chong, and M. A. Cazalilla, Phys. Rev. B **94**, 085414 (2016).